STUDY OF ALGORITHMS FOR ANALYSIS OF XRF SPECTRA TO AUTOMATE INSPECTION OF CARPETS

A Thesis
Presented to
The Academic Faculty

by

Laurent Mahuteau

In Partial Fulfillment
of the Requirements for the Degree
Master with Thesis Option in the
School of Electrical and Computer Engineering

Georgia Institute of Technology
December 2008

STUDY OF ALGORITHMS FOR ANALYSIS OF XRF SPECTRA TO AUTOMATE INSPECTION OF CARPETS

Approved by:

Professor Thomas E. Michaels,
Committee Chair
School of Electrical and Computer Engineering
Georgia Institute of Technology

Professor Jennifer E. Michaels
School of Electrical and Computer Engineering
Georgia Institute of Technology

Professor George J. Vachtsevanos
School of Electrical and Computer Engineering
Georgia Institute of Technology

Date Approved: August 2008

To all the people who supported me during my studies: my professors, family and friends.

ACKNOWLEDGEMENTS

There are many people to whom I would like to acknowledge and thank for their support in completing my thesis. First, I would like to thank my advisor Dr. Thomas Michaels for giving me the opportunity to conduct research under his guidance. It was a great experience to work on a project where such an interesting and challenging technology was at stake and a great opportunity for me to work with real experimental issues. I realized how careful and documented the measurements must be taken to yield confident interpretations and conclusions. Then, I would like to thank Dr. Jennifer Michaels who has always been willing to help me to analyze the data when I needed her and Dr. Vachtsevanos for being part of my thesis committee.

The state of Georgia is greatly acknowledged here for its financial support through state funding. Without their help, the project in which NASA and the Carpet Rug Institute (CRI) are interested in would not have been possible. NASA and CRI have both great expectations for using XRF technology for measurement of chemical concentrations during the carpet manufacturing process.

The support and help of Ler Gullayanon, PhD student working on detailed qualitative and quantitative XRF spectrum analysis, is also acknowledged. Ler helped me when I was desperate with very inconsistent results. I wish her good luck for the completion of her thesis, and hopefully my work will help her a little bit.

Last, but not least, I want to thank Shaw industries and especially Jeff Bowen for the time he dedicated to show us their on-site XRF instrument, help us to explain carpet mills issues and collect a representative variety of carpet samples.

TABLE OF CONTENTS

LIST OF TABLES

LIST OF FIGURES

SUMMARY

The objective of this thesis is to categorize carpet types according to their XRF spectra and verify if further classification of carpets is possible for use of an XRF analysis system in the carpet manufacturing line. This thesis consists of (1) implementing and studying effective algorithms for automated analysis of X-ray spectra, (2) comparing known algorithms for X-ray spectra analysis, and (3) implementing our own algorithm for classification of carpets spectra obtained for further fluorine online analysis of XRF inspected carpets. This research is intended for quick and accurate automated analysis of raw XRF spectra and matching analysis results to a database of XRF spectra of raw carpets. The research uses spectrum signal processing and spectrum analysis regarding efficacy of combined methods for XRF inspected carpets.

X-Ray Fluorescence is a key technology for detection of chemical elements. Fluorine is a key element for carpet's quality. Its very low concentration amount influences the carpet quality as well as its cost. Too much fluorine is costly whereas not enough threatens the carpet quality. XRF has been chosen to be a potential candidate to measure fluorine since it is a versatile tool for low concentration element detection. Due to specific XRF background spectrum for each different carpet type, carpet samples may need specific calibrations for further computation of carpet fluorine concentration. Automating the detection of the carpet type is intended to help in automating the XRF calibration.

In chapter one, the thesis summarizes previous work in terms of XRF analysis. Chapter two presents the measurement issues and reasons for the final measurement procedure. The last two chapters give further details of the data analysis methods and final results obtained.

CHAPTER I

INTRODUCTION AND LITERATURE REVIEW

1.1 History of X-Ray Fluorescence

The history of X-ray fluorescence dates back to the discovery of X-rays in 1895 by the German physicist Wilhelm Conrad Roentgen [2]. The use of X-rays in analytical chemistry began in 1913 when H. G. J. Mosley discovered a relationship between an element's atomic number Z and the reciprocal of the wavelength for each emission atomic spectral line, which are the transitions from a particular discrete energy level of an atom, to a lower energy state,

$$\frac{c}{\lambda} = a(Z - \sigma)^2 \tag{1}$$

where a and σ are constants for a given atomic spectral line [1].

In 1948, Friedman and Birks built the first XRF spectrometer, which created real prospects for analytical techniques to perform elemental analysis in all kind of samples. Since then XRF instruments have improved both in precision and accuracy. In fact, during the first decade after the implementation of the first XRF spectrometer, XRF instruments were capable of qualitative and quantitative analysis for elements with atomic numbers greater than 22 (Titanium). Now XRF spectrometers have progressed to the point where elements can be detected ranging from Beryllium (Z=4) to Uranium (Z=92) and in quantities ranging from few parts per million to high percentages [2].

XRF has been successfully applied to numerous applications including art verification, biology, biomedicine, pharmaceuticals, electronics (for RoHS compliance testing), environmental analysis, forensic science, geology and mineralogy, quality control processes and aerospace [3].

1.2 Physics of X-Ray Fluorescence

X-Ray fluorescence, or XRF, is a physical phenomenon corresponding to the emission of characteristic "secondary" X-rays from a material that has been excited by bombarding it with high energy X-rays or γ-rays [4]. XRF analysis covers the following range of energy or wavelengths:

$$E = 0.11 - 60 \text{ keV}$$

$$\lambda = 0.02 - 11.3 \; nm$$

with

$$E = \frac{h\,c}{\lambda} \tag{2}$$

$$c = 3.00 \times 10^8 \; m/sec \text{ and } h = 6.63 \times 10^{-}34 \; J \; sec$$

i.e.:

$$E[keV] = \frac{1.24}{\lambda[nm]} \quad [2] \tag{3}$$

When excited by the primary high energy X-rays, electrons are ejected from the sample atoms. When electrons from inner orbitals are ejected they leave holes that are filled by electrons from the outer orbitals. As electrons fall down from the outer orbitals to the inner orbitals, new X-rays are generated at energy difference between the two orbitals as seen on Figure 1. These secondary emissions are called X-ray fluorescence. Each element has its specific X-ray fluorescence emissions which correspond to specific energy differences between orbitals. Thus, every fluoresced X-Ray is part of the XRF signature of a specific element [5] and [4]. In addition to these specific XRF signatures, an X-ray energy continuum spectrum is emitted by the primary source due to the XRF instrument technology. The detailed X-ray energy continuum spectrum origin will be given in Section 1.4. All these X-rays are then detected by the detector of the XRF instrument and processed to display a spectrum. XRF spectra represent intensities (counts of X-rays) versus energies or wavelengths.

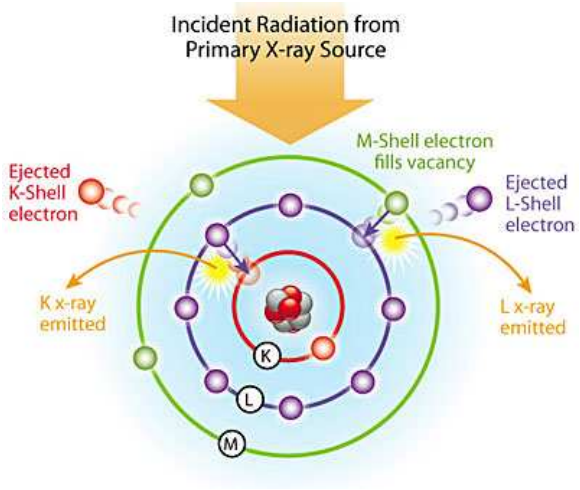

Figure 1: Physics of X-Ray Fluorescence (XRF) [1].

1.3 Energy dispersive XRF spectrometers

To detect these secondary X-ray emissions - X-Ray fluorescence - two different types of detectors are used: Energy dispersive and Wavelength dispersive X-Ray Fluorescence. Energy dispersive XRF and Wavelength dispersive XRF are two different types of detector technologies. The Energy dispersive XRF is suited to display intensities versus energies whereas the Wavelength dispersive XRF is suited for intensities versus wavelengths. We will only explain the technology for Energy dispersive XRF here since it is the technology employed in the instrument used for our studies. Energy dispersive XRF detectors provide a count of the number of photons detected at specific energies; whereas Wavelength dispersive XRF uses a diffraction method to separate various wavelengths of fluoresced X-rays [5].

Energy dispersive X-ray fluorescence relies on the detector and detector electronics to resolve spectral peaks due to different energy X-rays. It wasn't until the 1960's and early 1970's that electronics had developed to the point that high-resolution detectors, like lithium drifted silicon, Si(Li), could be made and installed in commercial devices. Computers were also a necessity for the success of Energy dispersive XRF and in many cases were as large as the instrument itself.

Regarding the hardware, Energy dispersive XRF is relatively simple and inexpensive

compared to other techniques. It requires an X-ray source, which in most laboratory instruments is a 50kV to 60kV, 50-300W X-ray tube. Low cost benchtop or handheld models have used radioisotopes such as Fe-55, Cd-109, Cm-244, Am-241 of Co-57 or a small X-ray tube. In an X-ray tube, electrons emanating from the heated cathode material are accelerated in an electrical field and shot against an anode. When they strike the anode material, electrons loose their energy through deceleration. A very small proportion of this energy (1 to 2 %) is converted into X-rays and the remainder is converted into heat [1].

The second major component is the detector, which must be designed to produce electrical pulses that vary with the energy of the incident X-rays. Most laboratory Energy dispersive XRF instruments use liquid nitrogen or Peltier cooled Si(Li) detectors, while benchtop instruments usually have proportional counters, or newer Peltier cooled PIN diode detectors, but historically sodium iodide (NaI) detectors were common. Some handheld devices use other detectors such as mercuric Iodide, CdTe, and CdZnTe in addition to PIN diode devices depending largely on the X-ray energy of the elements of interest. The most recent and fastest growing detector technology is the Peltier cooled silicon drift detector (SDD), which is available in some laboratory grade Energy dispersive XRF instruments.

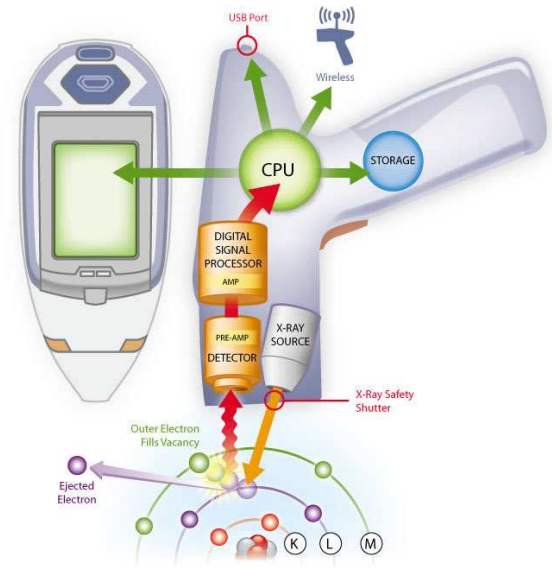

Figure 2: Hardware and software schematic of a typical handheld XRF instrument [1].

After the source and detector the next critical components are the X-ray tube filters,

which are available in most Energy dispersive XRF instruments. They are placed between the X-ray detector and the sample and between the sample and the X-ray tube. Their function is to absorb or transmit a specific range of energies. Secondary targets are an alternative to filters. A secondary target material is excited by the primary X-rays from the X-ray tube, and then emits secondary X-rays that are characteristic of the elemental composition of the secondary target. They are used to absorb count intensities in regions of interest while producing a peak that is well suited to exciting the elements of interest. Applicable secondary targets can yield a lower background and better excitation than filters but require approximately 100 times more primary X-ray intensity to effectively implement.

On the software side, data from the detector is usually preprocessed by a Digital Signal Processor and then sent to a CPU for further analysis. As shown on Figure 2, the CPU can either store the processed data or send it to a connected PDA, or to a PC via a USB port, serial port, or even with a wireless technology for the newest versions.

The Bruker KeyMaster Tracer II ^{TM} used in our studies is a handheld model using a small X-ray tube with a Silver (Ag) target which emits energies up to 40keV. It has an Energy dispersive XRF detector with a resolution of 39.91eV per channel. The instrument contains the latest technology high resolution Peltier cooled SiPIN detector. No specific filters have been added to the instrument we use. Still, if needed, one could be added to remove a portion of the energy spectrum to improve detection of trace elements of interest.

1.4 XRF spectra and classic analysis

1.4.1 XRF spectra characteristics

XRF spectra from the Energy dispersive XRF detector and the Digital Signal Processor represent intensities (counts of X-rays) versus energy channels. Each channel corresponds to a specific range of energies, the resolution of which depends on the instrument technology. The resolution of the XRF instrument used at Georgia Tech is 39.91eV per channel. The X-ray energies correspond to the energies electrons loose by decelerating when hitting the anode material. The distribution of the energies of all emitted X-rays ranges from 0 to 40keV. This results in a continuum spectrum called the "Bremstralhung" spectrum [2]. The

purpose of X-Ray fluorescence is the qualitative and quantitative determination of elements in a sample by measuring characteristic radiations. Yet, in addition to the fluorescence process, X-Rays can be scattered or absorbed by the material as shown on Figure 3. This

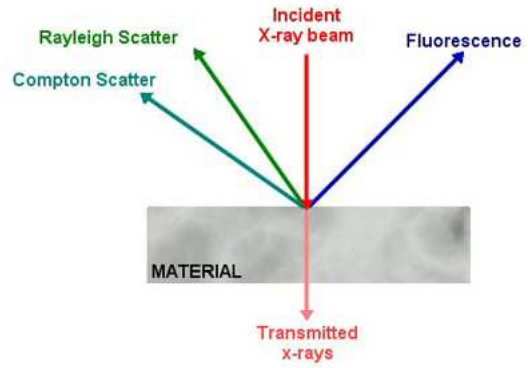

Figure 3: Different types of secondary X-rays emissions (fluorescence, transmission and scatterings) [2].

scattering can occur both with and without loss of energy (Compton and Rayleigh scatterings). Rayleigh scattering is an elastic scatter (without loss of energy). It reflects the Brehmstralhung spectrum to the detector. The Compton effect is an inelastic scattering that makes the X-rays lose energy. It makes a somewhat wider peak appear on the lower energy side of the element fluorescence peaks. For our instrument (with a Silver X-ray tube), the Compton peak from a carpet measurement spectrum is in the lower energies between the characteristic K_α energy transitions of Rhodium (Rh) and Palladium (Pd) which are drawn as vertical red lines in Figure 4.

1.4.2 XRF spectra classical analysis

Advanced digital signal processing software is not available for use with the portable XRF instrument used for our studies, and best results are often obtained when one relies on the operator's interpretation [6]. Spectra analysis consists in applying qualitative analysis to raw spectral counts versus channels. To develop accurate qualitative analysis methods, three classes of XRF spectrum analysis algorithms are typically used: (1) background spectrum estimation and filtering algorithms (2) noise filtering algorithms and (3) peak search methods. These will be discussed from a brief literature review next.

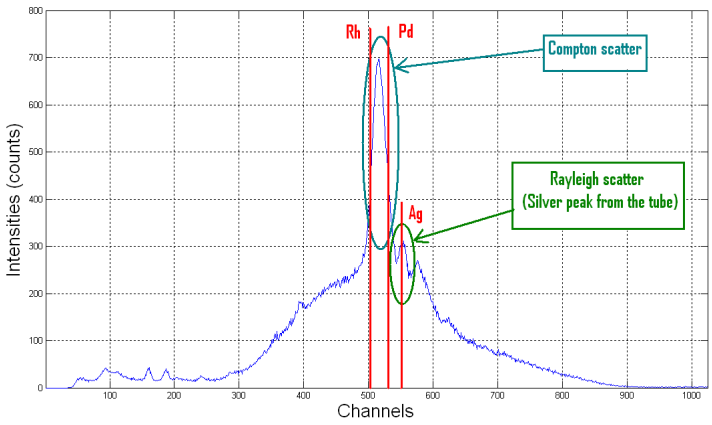

Figure 4: XRF background spectrum from a carpet measurement.

Background spectrum estimation and filtering algorithms

For heterogeneous and non-uniform samples, back scattered electrons and the Compton peak are primary concerns because they corrupt the XRF spectra and produce background counts that may perturb significant spectrum peaks from elements of interest. Thus, it is critical to develop calibrations and later make measurements on all specimens of the same type. Even when matching carefully the sample to calibrations standards from the same type of material, spectrum analysis and signal processing steps are required to accurately detect concentrations of various elements. This research uses the background spectra to aid in identifying the type of carpet sample for the purposes of automatically selecting the proper calibration standards from a calibration database. Further, background spectrum estimations will be performed and compared for effectiveness and accuracy.

Noise filtering algorithms

A second objective is to use algorithms to filter the noise from spectra to produce smoothed results from which detection of peaks is more precise. This spectrum filtering method can be applied to the raw spectrum or after the background estimation and filtering step, and performance metrics are developed to test the effectiveness of these filtering steps.

Peak search method

The final processing will involve the use of algorithms for automation of detection of the background elements in carpets samples. It will help in automating the detection of elements in the samples and ensuring that key information from the spectrum is not missed. This part will involve study of effectiveness of curve fitting of Gaussian functions, top hat filtering and spectrum derivation. And it will lead to implementation of best spectrum estimation using the most efficient technique.

1.4.2.1 Noise spectra filtering

Smoothing the spectrum is a necessary operation to get rid of noise. A Savitzky and Golay algorithm and moving average filter are known methods in the literature [4], [7], [8]. They have been implemented on our samples and typical results are shown in Figure 5.

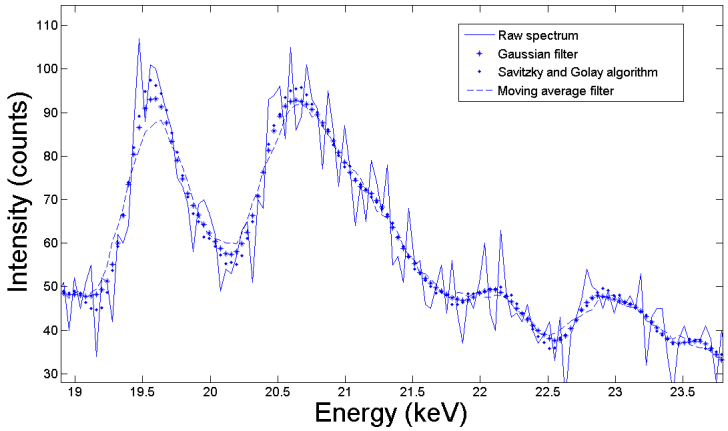

Figure 5: Raw spectrum and smoothed spectra obtained with smoothing methods for a 7 channel window width.

The Savitzky and Golay method performs a local polynomial regression on a distribution of a certain width to determine the smoothed value for each point. Other smoothing methods, such as moving average and Gaussian filters, involve a convolution with the spectrum. The filters have a gain equal to one, and are symmetric in relation to the point to smooth. Results shown in Figure 5 and Table 1 are typical of what is obtainable with these methods. Gaussian filter best tracks the original spectrum, and the difference in counts with the raw

spectrum is lower than the Savitzky and Golay algorithm or the moving average filter for a width of 5 or 7 channels.

Table 1: Noise filtering - Error (difference of counts per channel between smoothed spectrum and the raw spectrum) for each method.

Size of the filter window	5 channels	7 channels	9 channels	11 channels
Savitzky-Golay algorithm	2.118	2.299	2.179	2.285
Gaussian filter	1.625	1.962	2.1974	2.421
Moving average filter	2.150	2.408	2.6948	2.989

1.4.2.2 Estimation of background spectra

Peak stripping and polynomial background estimation discussed in the literature [7], [4] and [9] are methods which were implemented and tested, and results are shown in Figure 6.

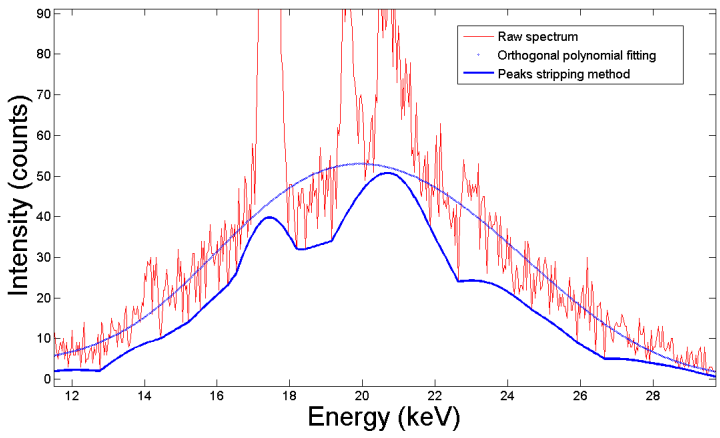

Figure 6: Background estimations using peak stripping and orthogonal polynomial estimation methods for a typical carpet sample containing Molybdenum.

The peak stripping method estimates the background from its lowest limit as shown in Figure 6. The orthogonal polynomial background estimation method, introduced by Steenstrup [9], smoothes noise errors. As compared in Table 2, the error between the raw spectrum and the spectrum processed with the peak stripping method is greater than with the polynomial orthogonal background estimation one. Once estimation method is performed, we filter the background by subtracting it from the spectrum.

Table 2: Errors between raw spectrum and processed spectrum for peak stripping and orthogonal polynomial estimation method.

Background estimation method	Error
Peaks stripping method	9.12 counts/channel
Orthogonal polynomial background estimation	6.58 counts/channel

1.4.2.3 Peaks search

As shown in Figure 7, after the background spectrum is estimated and filtered, and the processed spectrum has been smoothed, peaks are readily visible and these can easily be detected to determine which elements are in the sample.

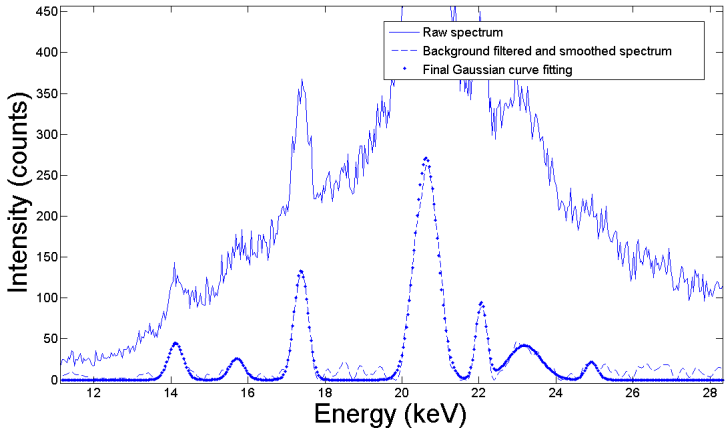

Figure 7: Automated peak search method for a bare carpet containing traces of Molybdenum.

Figure 7 shows results obtained from a peak search method. For this example, the peak stripping method [9] and a Gaussian filter have been used respectively as background estimation and smoothing method. Use of other possible combinations of methods have not been displayed here for the sake of conciseness. The intensity and position of peaks can be determined using a Gaussian curve fitting method [4], [7], [10], where a threshold is applied to process the data above this threshold [11]. Although this step is not shown, results obtained are in agreement with the sample analyzed. We detect strong peaks from Strontium (Sr) from the backing of the carpet, Molybdenum (Mo) which was added to the carpet prior to the measurement, Rhodium (Rh) and Silver (Ag). In addition to curve

fitting methods, filtering the spectrum with hat filters or differentiating the spectrum, once or twice, are other ways to process spectra, and our trial results match work completed in the literature [7], [4]. To ensure better reliability in the results, one solution, not displayed here, consists in applying a top hat filter to the smoothed spectrum to locate most probable peaks and then apply a Gaussian curve fitting method. Finally, the superposition of these three methods, summed up by the model presented in Figure 8, ensures that peaks detected are actual peaks of elements and not from the background spectrum.

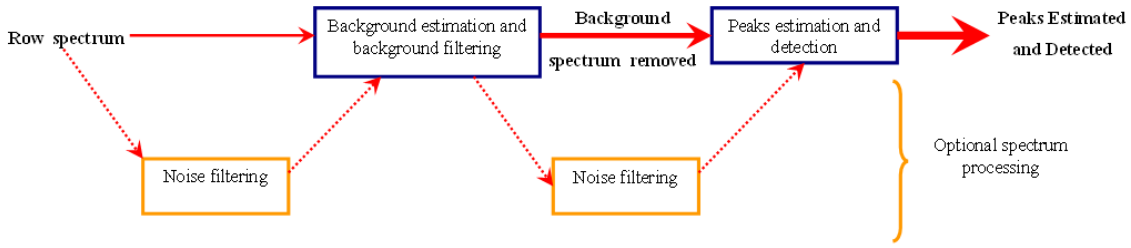

Figure 8: Model proposed for analysis of XRF spectra.

CHAPTER II

EXPERIMENTAL METHODS

2.1 Instrumentation

The XRF analyzer is the key instrument for measurements made in this study. This instrument is a handheld XRF device, weighing around 3 lbs., manufactured by KeyMaster Technologies (Bruker AXS). Because the instrument does not operate with a vacuum between the sample and the detector, it can only detect elements above Titanium (atomic number Z=22) on the periodic table. This is because low energy X-Rays from elements below Titanium ionize completely in air before reaching the detector. KeyMaster Technologies provided the instrument with a Personal Digital Assistant (PDA), an instrument stand and PC based data acquisition software. The complete system with the data acquisition PC is shown in Figure 9.

Figure 9: Setup and material used for experiments: XRF instrument, PC used for data acquisition and stand supporting carpet samples.

For practicality, the X-Ray instrument is used in a stand with the instrument pointing upwards. The XRF instrument protruded through a plastic plate placed on top of the stand, on which carpet samples were faced with the side to be measured oriented down. A hole (dimensions: $4 \times 2 \times 1$ inches) was machined in the upper plate to allow the X-Ray instrument to be adjusted in stand-off distance to the sample.

Two options are offered by the instrument manufacturer to acquire the data after a measurement is completed, either with a PDA or the PC based data acquisition software. The PDA is intended for use when the XRF instrument is used remote from a host computer. The PC acquisition is more suited for laboratory measurements and subsequent data analysis on a PC. Thus, for our work we only used the PC data acquisition software. The user interface for the PC based data acquisition software PXRF, supplied by KeyMaster, is presented in Figure 10. Using this software, the data are saved as .csv files (comma separated variable). We then use Matlab to extract the data from these .csv files, knowing their specific format.

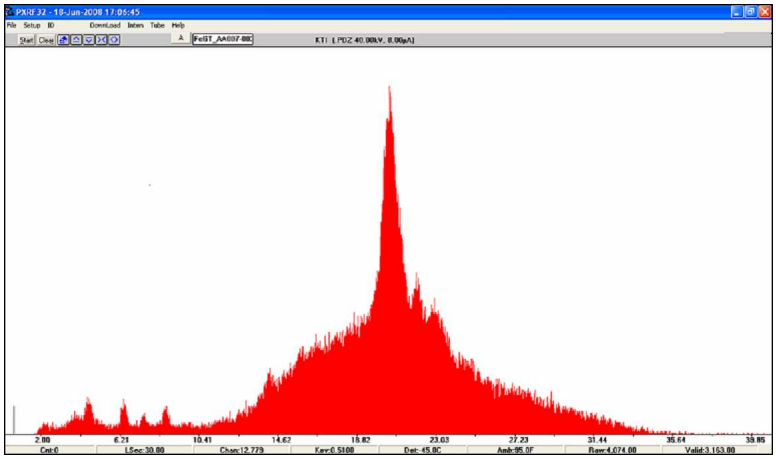

Figure 10: PC interface and spectrum display used for data acquisition with the XRF handheld instrument which has a fixed resolution of 39.91 eV per channel.

In summary, the experiments required four main resources: (1) the XRF hand held instrument (key resource for measurements), (2) an assorted variety of carpet samples, (3) PXRF software for data acquisition, and (4) Matlab for data analysis. Matlab programs were written as a suite of analysis algorithms and other software tools for carpet classification.

2.2 Specimens analyzed

The carpet samples tested for this study were raw carpet samples manufactured by Shaw industries. They represent a large variety of residential and commercial carpet types that will be used later for the project and to which taggants will be added for quality control of

Fluorine concentration, which is a follow on goal to this project.

Only a small proportion of commercially available carpet types were tested in this study, but the goal was to develop a classification technique using a representative cross section of the most common carpet types. Samples were chosen from carpet types which had visual features that might affect XRF measurement results, which included a total of 49 residential and commercial carpets. Specific mill characteristics associated with these carpets are (1) color, (2) texture, (3) pile height, (4) density, (5) weight and (6) backing type. Table 3 gives the different mill characteristics of a few of the samples. For more details, the entire database and all characteristics are given in Appendix A.

Sample Units (if applicable)	**Color**	**Texture**	**Pile height in**	**Density oz/yd^2**	**Weight oz**	**Backing**	**Code**
GT FS006	101	F	1.03	2045	58.5	Soft	51681
GT FA016	305	F	0.51	3106	44	Action	51112
GT AA022	303	A	0.12	7800	26	Action	77353
GT FA036	154	F	0.67	1574	29.3	Action	51033
GT FS039	121	F	0.38	3316	35	Soft	59219
GT FS049	106	F	0.69	2546	48.8	Soft	51592

Table 3: Mill characteristics of a few carpet samples collected.

In Table 3, we either use figures to describe carpet characteristics or labels when the characteristics are not quantifiable. All carpets names begin with "GT". The next two letters represent the type of texture and the type of backing. The type of texture is either "F" or "A". According to the standards and requirements of the Department of Housing and Urban Development [12], an "F" texture type of carpet is made of Cut Pile Heat set - Plied. This Texture F includes Single level or multilevel cut or cut-and-loop pile, made from balanced heat set and plied yarns. An "A" textured carpet is made of Level or Texture Loop. This texture includes level uncut piles with a pile height differential of not more than 1/16". The second letter designator is for the type of backing, i.e., either an Action backing (denoted as "A") or a Soft backing (denoted as "S"). The final number is the primary key to differentiate between carpets, for example, the carpet labeled "GT FS011" is the 11th carpet referenced in the database, it is made of Texture F and joined with a Soft backing. Among the above carpet types, we have further distinguished three visual categories:

- non-uniform carpets (carpets with patterns)
- uniform carpets with non uniformly distributed fibers
- uniform carpets with uniformly distributed fibers

The above three visual categories are subjective definitions set up for our studies. For example, Figure 11 shows a carpet type from each of the above categories to illustrate our classification method. In summary, the left photograph is an example a non-uniform carpet with patterns and relief, the center photograph is an example of a uniform carpet with non-uniformly distributed fibers where the fibers are loose and not in the same direction, and the right photograph is of a uniform carpet with uniformly distributed fibers where the top fibers are evenly distributed and in the same direction. Depending on the type of carpet we analyze, our studies will show that the measurements are influenced according to the carpet category being inspected.

Figure 11: Examples of the three different types of carpets - From left to right, carpet "GT FS041" is non uniform (with patterns), "GT FS039" is uniform and has fibers uniformly distributed and "GT FA048" is uniform and has fibers non uniformly distributed.

2.3 Experimental settings

2.3.1 XRF instrument settings

The instrument we are using for experiments has flexibility in terms of current and voltage applied to the the Silver (Ag) tube of the hand held instrument. As mentioned before in Chapter 1, the XRF instrument has a fixed resolution of 39.91 eV per channel with 1024 channels over 40kV. Six options or combinations of current and voltage for the X-Ray tube are available to the user for set up of the instrument. These are, as shows Figure 12: 30kV and $10\mu A$, 35kV and $8\mu A$, 35kV and $4\mu A$, 40kV and $8\mu A$, 40kV and $3.6\mu A$, or 40kV and

$10\mu A$. The tube voltage corresponds to the range of energy transitions. The higher the

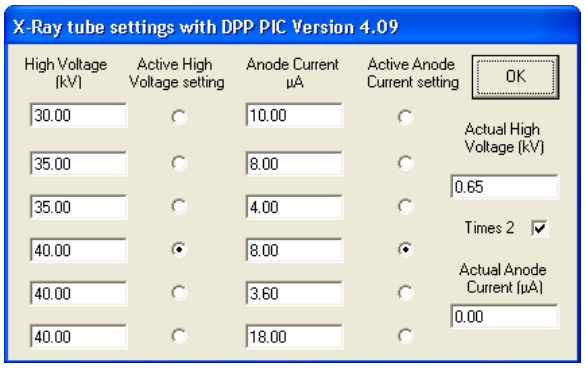

Figure 12: Display of the interface to choose the different settings possible for the instrument.

voltage applied to the tube, the higher are the energies of the primary X-rays and the bigger is the detectable elements range. Further, for a voltage level lower than 40kV, the detector energy range is reduced in number of channels since the per channel sensitivity of the instrument is fixed. Thus, we set the voltage to its maximum for our studies to have as high of a detection range as possible.

The tube current influences the number of X-ray counts detected. A higher current produces more X-Rays and hence more counts. Specifically, when more electrons are beamed towards the target, more X-Rays are generated, and a greater number of counts reach the detector from the sample. The advantage of a high current versus a low current is improved accuracy, i.e. fewer count variations for the same measurement time. Higher current has the drawback of more quickly heating up the instrument. We used a compromise between measurement accuracy (low noise errors) and reasonable temperature conditions by choosing a current setting of $8\mu A$. Thus, final settings were 40kV for the tube voltage and $8\mu A$ for its current.

2.3.2 Sample preparation

The samples tested are listed in Appendix A. They were all prepared and measured the same way. Knowing that the carpets are not uniform and especially that for some of them the fibers are not uniformly distributed, we brushed the carpets in one direction and placed them in a plastic bag for the measurements. Once brushed and inserted in the bag, the

sample is placed face down on the plastic sample stand and held in place with a weight of approximately one pound as shown on Figure 13. The brushed direction of the fibers was always oriented in the same direction on the sample stand.

Figure 13: Preparation of the carpet samples - Carpets are brushed and inserted in a tight plastic bag. The direction on which we brush the carpet and in which we insert it into are the same.

2.4 Measurement tests

It is important to obtain good accuracy of actual counts from various spectral peaks in order to determine the concentrations of elements present in carpet samples using XRF. In fact, if variations are too great, intensity counts and thus computed percentages of low concentration elements in samples will be very imprecise. The test procedures described in this section were developed to minimize scatter in our overall measurement results and the remove as much noise from XRF spectra as possible. As is listed in our database, several XRF spectra were acquired under different conditions to determine several measurement aspects that affected measurement repeatability. For repeatability tests under various temperature and XRF instrument standoff conditions, we choose a uniform carpet, because, as we will show in Chapter 4, uniform carpets provide the most consistent measurements. Several important parameters had to be tested to ensure a good basis for further analysis:

- Ambient temperature of the chamber of the XRF instrument
- Distance between the detector and the top fibers
- Carpet uniformity
- Measurement reproducibility and consistency

Experimental results for each of the above items are detailed in the following sections. In all these cases, to make sure that we tested only one parameter at a time, all other parameters were kept constant for each individual test.

2.4.1 Influence of the ambient temperature of the instrument

Instrument ambient temperature has a significant affect on instrument accuracy. As mentioned in [13], experimental issues due to temperature are not negligible for XRF measurements. Two different temperatures for the XRF instrument are displayed on the PC user interface, Figure 10, (1) the detector temperature and (2) the ambient temperature at the open end of the XRF instrument near the sample. The instrument has controls to keep the temperature of the detector nearly constant between -45°F to -45.5°F. Specifically, the high resolution SiPIN diode detector is Peltier cooled to this temperature range, and does not vary enough during normal use of the instrument to produce inaccurate results. On the contrary, the ambient temperature of the instrument (the temperature of the air in the chamber of the instrument near the sample) varies substantially between 78°F to 116°F as the instrument heats up during use. This is due to the fact that 98% of the energy of the tube is converted to heat, but only about 2% is actually converted into X-rays. Additionally, the electronics inside the XRF instrument heats up, including the X-Ray tube, and also contributes to this temperature rise. For our laboratory measurements, we have noticed that an upper bound for the ambient temperature is around 120°F, after which a steady state temperature is reached. Typically, for a 30 second measurement, the temperature rise is approximately 0.5°F for a tube setting of 40keV and $8\mu A$. To test the influence of the ambient temperature, several measurements were made at the same spot on carpet "GT FA011". These measurements were taken one after the other to make sure that the temperature increased steadily above 78°F. The carpet position was not changed and we kept recording every 30 seconds until the temperature reached 110°F. Experimental results are given in Figures 14 and 15.

As is shown in Figure 14, the higher the ambient temperature, the less consistent are the measurements. Specifically, a higher temperature produces an increasingly lower number of

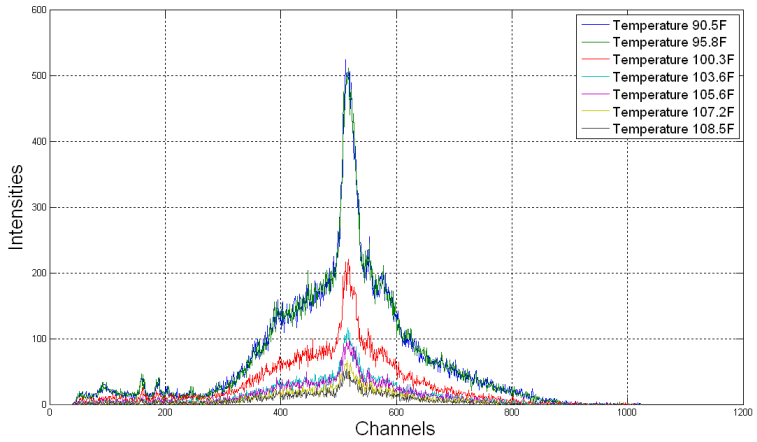

Figure 14: XRF spectra of the same spot of the carpet "GT FA011" and acquired at temperatures ranging from 90 °F to 110 °F.

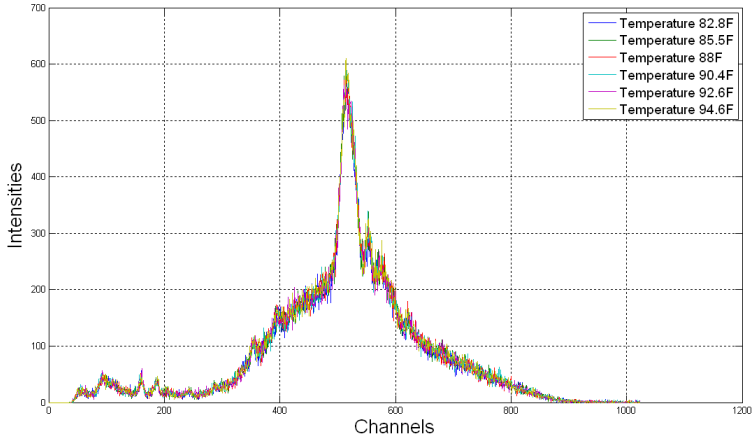

Figure 15: XRF spectra of the same spot of the carpet "GT FA011" and acquired at temperatures below 96 °F.

counts for the same spot on the carpet. However, we notice that below a certain temperature threshold, which we estimate at around 96 °F, this temperature affect diminishes such that the spectra are on top of each other as is shown in Figure 15. Thus, for measurements below 96 °F, the spectra are fairly repeatable. This temperature threshold is explained by the fact that the electronics, including the detector and readout unit, are insensitive to temperature only within certain limits, and the useful range of operation for our instrument is below 96 °F.

2.4.2 Influence of the distance detector - top fibers

To assess the influence of the distance between the X-ray detector and the top fibers, we tested and compared the averaged measurements for four different distances. The temperature for these measurements was kept below 96 °F. The four different distances correspond to the spacing between the front of the XRF instrument and the sample: 0", 0.125", 0.25" and 0.375". At each distance we averaged measurements from five different spots on the sample.

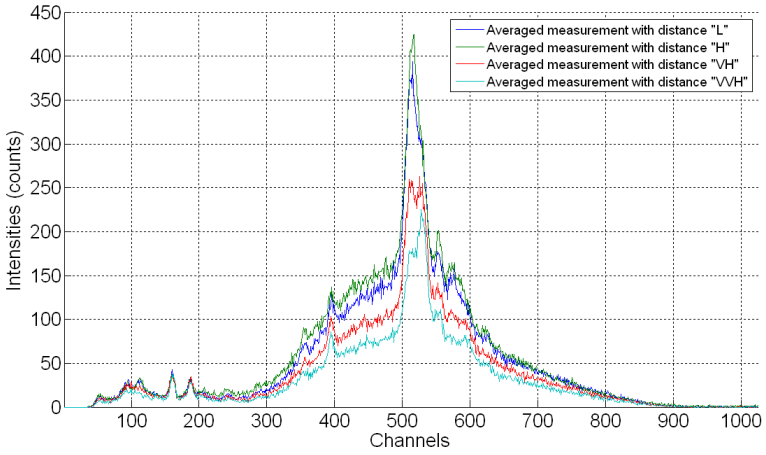

Figure 16: Plots of the averaged spectra of the carpet "GT FS049" measured with distances of 0, 0.125, 0.25 and 0.375 inch (labeled "L", "H", "VH" and "VVH") between the X-ray detector and the top fibers.

These different averaged measurements are labeled "L", "H", "VH" and "VVH", for distances respectively equals to 0", 0.125", 0.25" and 0.375". As shown on Figure 16, the spectra have very close shapes (except for the Compton peaks which are slightly changing for a distance above 0.25"). Additionally, as shown in Table 4, the closer the carpet is to the X-ray detector, the more counts are detected. This is explained by the fact that since the electron flux to the target is fixed for a specific tube setting, then the actual X-Ray flux produced is also constant; however, as the gap increases between the sample and the detector, the probability of X-Rays reaching the detector is reduced since they attenuate with distance.

A straightforward way to deal with the issues of differences in total counts and variations

Label	L	H	VH	VVH
Distance in inches	0	0.125	0.25	0.375
Total Counts	58,194	52,879	40,755	31,703
Total Counts / Channel	56.83	51.64	39.80	30.96

Table 4: The total counts per channel for XRF measurements of carpet sample "GT FS049" below 96 °F increases while the distance between the X-ray detector and the top fibers decreases.

in the Compton peak, as experimental parameters are varied, is to compare measurements with an identical distance between the detector and the carpet. Using this methodology, measurements will be comparable and further differentiation and classification among carpets will be feasible. Thus, for our experiments, we use a 0" standoff distance. Specifically, the sample is prepared as explained in Section 2.2, i.e. it is placed face down on the plastic sample stand and compressed on the stand by applying a weight of approximately one pound, and the stand is adjusted in height so that the top of the XRF instrument touches the plastic bags used to prepare the samples.

2.4.3 Influence of the carpet uniformity

Another issue with analyzing samples via XRF instruments is the homogeneity of the sample analyzed. In fact, the more homogeneous, the better and the more consistent are the raw data. Visually speaking, carpets have a heterogeneous look. Measurement variations within a same carpet can vary substantially due to non flat surfaces and more or less dense carpet locations in terms of fibers. Apart from the influence of the distance between the detector and the carpet, the direction of measurement, and the temperature, the nature of the carpet itself is a factor to take into consideration when determining measurement consistency. For certain carpet samples, the fibers are visually not uniformly distributed and the measurements are inconsistent from one spot to another. For this reason, as explained in the description of the samples analyzed, we distinguished three types of categories of carpets: (1) non uniform carpets (patterns on the carpets), (2) uniform carpets with non uniformly distributed fibers and (3) uniform carpets with uniformly distributed fibers.

The non uniform carpets include all the carpets which have patterns and relief. The different patterns cause the distances to vary between the carpet and the detector. Thus,

electrons are not returned the same way from one pattern to another. To determine whether patterns would influence measurements consistency, a carpet within which different patterns are built have been analyzed on the spots with different patterns. Figure 17 shows the mea-

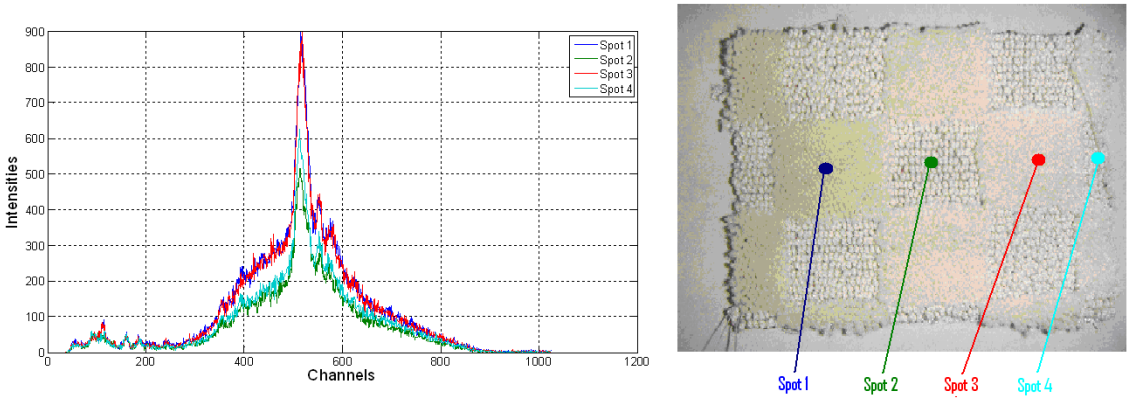

Figure 17: Plot of the different measurements from carpet "GT FS038" at approximately 93 °F (± 1 °F). Inconsistent measurements are due to more or less high patterns of the carpets.

surements acquired. Results actually show that the patterns do influence the measurements. In Figure 17, spectra drawn in blue and red colors are measurements for spots made of cut pile whereas spectra drawn in green and light blue colors are measurements for spots made of loop pile. Because the spots made of loop pile are tufted shorter, i.e. further from the detector, than the spots made of cut pile, fewer electrons are returned in the detector and fewer counts are recorded for the measurements for spots made of loop pile than for the measurements for spots made of cut pile.

For non uniform carpets, results are inconsistent because of the carpet nature itself. As a result, since raw data from these carpet measurements depend on the carpet locations, they were not kept as part of our final database. For uniform carpets, as shown in Figure 18, results are more consistent. These uniform carpets were kept for our final database. Among uniform carpets, measurement consistency for these carpets is still different for one sample to another. Their measurement consistency will be quantified in Chapter 4.

2.4.4 Measurement reproducibility

The measurement reproducibility due to instrument drift is another issue that is different from measurement variations due to external parameters such as temperature, distance

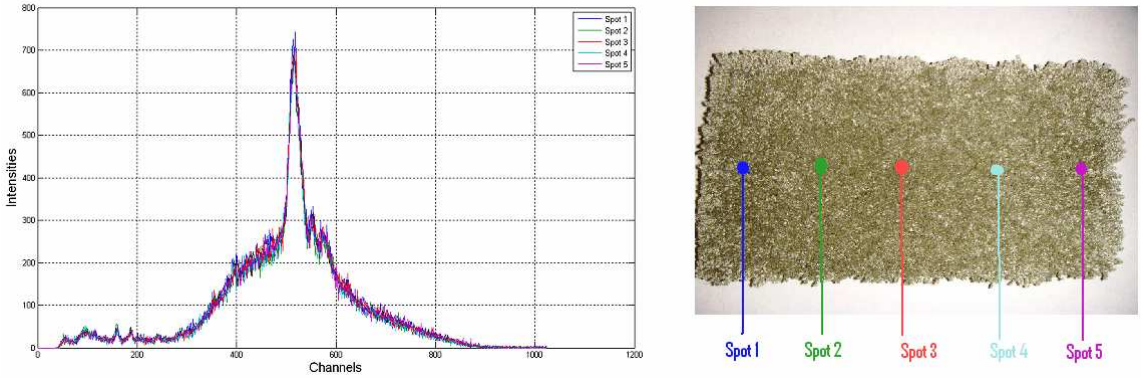

Figure 18: Plot of the different measurements from carpet "GT FS014" at approximately 90 °F (± 1 °F). Fairly consistent measurements are attributed to uniformity of the carpet.

between the detector or sample uniformity. Regarding this issue, the questions raised were: (1) Will we get identical measurements with negligible (or little) variation for the same spot of the same sample and constant temperature over time? (2) Is this variation due to measurement reproducibility more important than the variation due to others parameters?

Regarding the above mentioned issues, purposely, no raw data have been displayed in this section because it is not possible yet to draw any conclusions. However, these questions will be clarified in Chapter 3 when methods for calculation of measurement variations and experiment results will be explained.

2.5 Final measurement procedure

To ensure correct measurement reproducibility and to be confident in measurement reproducibility and consistency, database measurements have to be realized with the same well characterized procedure. Tests previously explained have been our guidelines to set up our final measurement procedure. Characteristics for the final procedure are the following:

- Instrument tube settings
- Distance between the X-ray detector and the sample top fibers
- Measurement time
- Uniformity and homogeneity of the surface beamed by the X-rays
- Measurements of several spots for the same carpet
- Ambient temperature of the instrument chamber

In terms of voltage and current settings, the instrument tube is set to be used with 40kV and 8μA. Regarding the previous parameters we tested and the conclusions those tests drove us to, distance between the detector and the instrument is kept constant as low as possible. The ambient temperature is kept below the temperature threshold estimated at 96 °F.

The list of carpets collected at Shaw industries is given in Appendix A. They are of three different types: (1) non-uniform carpets (carpets with patterns), (2) uniform carpets with non uniformly distributed fibers and (3) uniform carpets with uniformly distributed fibers. Yet, the visually non uniform carpets (ie. the carpets which have patterns) are not used for the rest of the study because of the inconsistent raw data they yield. Thus the final database of carpets kept and analyzed using this final procedure consists of (1) uniform carpets with non uniformly distributed fibers and (2) uniform carpets with uniformly distributed fibers. Eventually, before measurements the final carpets listed in Appendix B are wrapped in a thin plastic bag and held using a weight as explained in Section 2.2 to make their fibers appear as uniformly distributed as possible.

Following this procedure, for the 40 final carpets listed in Appendix B, five different measurements of five different locations are acquired. Using several different locations helps diminish the effects of the noise count variations by smoothing the spectra measurements. Besides, a measurement average of five different carpet locations is more reliable and more representative of the analyzed carpet type. Finally, for easy data handling, a number is attributed to each of these 40 carpets (a matching table between carpet numbers and carpet names is given in Appendix B).

CHAPTER III

DATA ANALYSIS AND SIGNAL PROCESSING

In this chapter, specific data analysis techniques are used for XRF spectra measurement analysis. Details about signal and data processing algorithms are provided.

3.1 Notation

3.1.1 Spectrum data set

At first, consider a spectral data set acquired for any particular sample for any particular spot. It consists of a total of N intensities for its N respective channels. For data analysis purposes, this set of data is handled as a row or column vector designated by X. This vector has N channel entries corresponding to N intensity counts. If n is the channel subscript, the intensity count for the n^{th} channel is designated by $X(n)$. Counts being logically positive and the number of channels being N, the following properties define a set of any spectral data:

$$X(n) \geq 0 \text{ for all } n \text{ such that } 1 \leq n \leq N$$

3.1.2 Spectral database

Now consider the spectral database. As Chapter 2 indicates, the database consists of measurements taken from five different locations among 40 different carpet samples which translates to a total of 200 measurements. The XRF sintrument settings and procedures used for these measurements have been described in Chapter 2. All measurements were made below the critical ambient temperature threshold of 96 °F, above which substantial measurement variations occur. Next, the chosen format used for cataloging the database is a three dimensional matrix X. Carpets numbers, carpet measurement numbers and channels numbers are respectively stored in the first, second and third dimension of this matrix. The intensity counts of the n^{th} channel of the k^{th} measurement of the i^{th} carpet is stored

in $X(i,k,n)$. The format and notation is described by:

$$X(i,k,n)$$

$$\text{such as: } 1 \leq i \leq C,\ 1 \leq k \leq M \text{ and } 1 \leq n \leq N$$

$$\text{with: } C = 40,\ M = 5 \text{ and } N = 1024$$

The notation above is different from that given in Section 3.1.1. The "Spectrum data set" notation, given in Section 3.1.1, is used when referring to any spectral data set. When referring to a specific database one, the "Spectral database" notation is used. For the rest of the thesis, when using this three dimensional matrix notation, reference will be made to a specific carpet in the database. If a one dimensional vector of data is used, reference to any spectral data set will be pointed out.

3.2 Measurement consistency

A study was conducted to determine the factors affecting measurement consistency. Specifically, measurement variations were characterized as a function of parameters listed in Chapter 2. Of specific interest is quantifying the affect of measurement reproducibility on our subsequent analysis results. This was accomplished by comparing results from several measurements acquired under similar conditions. Once a consistent measurement protocol was developed, we will then proceed to use it for the remaining spectra comparisons of the various carpet samples.

Both qualitative and quantitative methods were used to evaluate the consistency of measurements. The qualitative method is a simple visual comparison of spectral plots to determine the differences. The quantitative method consists in applying standard metrics for the sole purpose in determining, numerically, the differences between spectra [14].

A straightforward way to quantitatively compare a set of two spectra X_1 and X_2 at the same channel is to compute the normalized difference d_{12} between their channel count

values defined for each channel k:

$$d_{12}(k) = \begin{cases} \frac{\sqrt{(X_2(k)-X_1(k))^2}}{\frac{X_1(k)+X_2(k)}{2}}, & \frac{X_1(k)+X_2(k)}{2} > 0, \\ 0, & \text{otherwise}, \end{cases} \tag{4}$$

Next, the normalized standard deviations of measurements $X1$ and $X2$ are defined for each channel k as:

$$s_1(k) = \begin{cases} \frac{\sqrt{(X_1(k)-\frac{X_1(k)+X_2(k)}{2})^2}}{\frac{X_1(k)+X_2(k)}{2}}, & \frac{X_1(k)+X_2(k)}{2} > 0, \\ 0, & \text{otherwise}, \end{cases} \tag{5}$$

$$s_2(k) = \begin{cases} \frac{\sqrt{(X_2(k)-\frac{X_1(k)+X_2(k)}{2})^2}}{\frac{X_1(k)+X_2(k)}{2}}, & \frac{X_1(k)+X_2(k)}{2} > 0, \\ 0, & \text{otherwise}, \end{cases} \tag{6}$$

These two metrics are based on the difference and standard deviation between two measurements. However, since the raw data are absolute intensity counts, a normalization method was required to use these more standard metrics to make comparison of measurement variations possible. This normalization method consisted in normalizing by the average of the measurement counts. The normalized difference between measurements and the normalized standard deviation of each measurement relative to a whole set are the basis of methods for understanding the consistency of measurements and is used later in Chapter 4.

3.3 Consistency of measurements from different locations on the same carpet

To characterize consistency of measurements from different positions on the same carpet, the difference between the measurements and the standard deviations relative to the whole set are used. To quantify measurement consistency across carpet, measurement spectra taken from five different locations on a carpet specimen are used. The difference between intensity counts of measurements k_1 and k_2 of carpet sample i at channel n is defined as $D1(i, k_1, k_2, n)$ such that:

$$D1(i, k_1, k_2, n) = \begin{cases} \frac{\sqrt{(X(i,k_1,n)-X(i,k_2,n))^2}}{\frac{1}{M}\sum_{k=1}^{M} X(i,k,n)}, & \frac{1}{M}\sum_{k=1}^{M} X(i,k,n) > 0, \\ 0, & \text{otherwise}, \end{cases} \tag{7}$$

Alternatively, $D2(i,k,n)$ is the standard deviation of measurement k of carpet sample number i relative to the set of the five different measurements of carpet i. It is defined for channel n such that:

$$D2(i,k,n) = \begin{cases} \frac{\sqrt{(X(i,k,n) - \frac{1}{M}\sum_{k=1}^{M} X(i,k,n))^2}}{\frac{1}{M}\sum_{k=1}^{M} X(i,k,n)}, & \frac{1}{M}\sum_{k=1}^{M} X(i,k,n) > 0, \\ 0, & \text{otherwise}, \end{cases} \tag{8}$$

We recall that the subscripts i (carpet sample subscript), k, k_1 and k_2 (carpet measurement subscripts) and n (channel subscript) are greater than or equal to one and respectively less than or equal to $C = 40$, $M = 5$, and $N = 1024$. The matrices $D1$ and $D2$ contain normalized measurement variations either using the difference between two carpet measurements or the standard deviation of a carpet measurement relative to the set of the five measurements of the same carpet.

From these two data sets $D1$ and $D2$, the mean of the normalized measurement variations are computed for the different spots on the same carpet. It yields two new data sets $D1_{total}(i,n)$ and $D2_{total}(i,n)$ which characterize measurement consistency across carpet and that are defined for each sample i, at channel n as:

$$D1_{total}(i,n) = \frac{1}{M}\sum_{k_1=1}^{M} \frac{1}{k1}\sum_{k_2=1}^{k1} D1(i,k_1,k_2,n) \tag{9}$$

$$D2_{total}(i,n) = \frac{1}{M}\sum_{k=1}^{M} D2(i,k,n) \tag{10}$$

The smaller the actual numerical values $D1_{total}(i,n)$ and $D2_{total}(i,n)$ the more consistent are the measurements across carpet i for channel n. Using the data sets $D1_{total}$ and $D2_{total}$, comparison of measurement consistencies across carpets may now be made. Results of the carpet measurement consistencies will be detailed in Chapter 4. In the next section, discussion about algorithms used to compare two XRF spectra measurements and, later, to differentiate database carpet sample measurements is provided.

3.4 Methods and algorithms for spectra differentiation

3.4.1 Absolute spectra comparison

The first method used to compare spectra consists of evaluating the spectra total count numbers averaged by their total number of channels. To compare one spectrum to another, a straight forward difference between their averaged total count numbers is used. This difference is an overall value characterizing total counts spectra variation and is designated as $D_{TotalCounts}$:

$$D_{TotalCounts} = \left| \frac{1}{N} \sum_{n=1}^{N} X_1(n) - \frac{1}{N} \sum_{n=1}^{N} X_2(n) \right| \tag{11}$$

This absolute spectra comparison method gives significant results as we will see in Chapter 4. Still, using the total number of counts is a constrictive method. For instance, it obscures the shape characteristics such as relative peak heights and background spectrum. Relative spectra comparison methods presented in the next section preserve more of the overall spectral features.

3.4.2 Relative spectra comparison

Four different types of relative spectra comparison are explained in this section. Although, these comparison methods are mathematically different, we will see in Chapter 4 that they lead to equivalent results when using them for database matching purposes.

3.4.2.1 Frequency Domain Differencing

Spectrum Differencing is an application of Time Domain Differencing to spectral data as described in literature [15] and [16]. In our later analysis, we will use this method to compare two signals as function of energy channel. The comparison method of these signals is a simple substraction and produces a comparison metric $D(n)$ which is independent of the amplitude of the original signals X_r and X_m:

$$D(n) = \widetilde{X_m(n)} - \alpha X_r(n) \tag{12}$$

where:

$$\widetilde{X_m(n)} = \frac{X_m(n)}{\sqrt{\sum_{n=1}^{N} X_m(n)^2}} \tag{13}$$

$$\alpha = \frac{\sum_{n=1}^{N} \widetilde{X_m(n)} X_r(n)}{\sum_{n=1}^{N} X_r(n)^2} \tag{14}$$

The measured signal X_m is scaled to unity energy, and α, the scale factor of the reference signal, is calculated to minimize the mean squared error between $\widetilde{X_m(n)}$, the unity energy measured signal, and the scaled reference signal. Thus, $D(n)$ is an amplitude-independent measure of the difference between the signals. The energy of $D(n)$ within a specified window, referred to here as the residual energy, is calculated as a measure of this difference by:

$$E = \sum_{n=n1}^{n2} D(n)^2 \tag{15}$$

where $n1$ and $n2$ are the first and last subscripts of the selected window. The lesser the value of the residual energy E is, the closer the match is between the two spectra. This metric will be used later when we match measurements to previously obtained database values.

3.4.2.2 Normalized Energy Differences

An other way to compare the spectra shapes consists of evaluating the difference between two normalized spectra. To compute these differences, three main steps are followed: (1) the spectra X_1 and X_2 are normalized, (2) the squared difference between the intensity counts of the two normalized spectra is computed for each channel n and (3) those squared differences are accumulated within a specified window of length N.

Two different spectrum normalization methods are used. The first uses the integral of the total spectrum counts averaged by the total number of channels as the normalization factor:

$$E_1 = \sum_{n=1}^{N} \left(\frac{X_1(n)}{\frac{1}{N}\sum_{k=1}^{N} X_1(k)} - \frac{X_2(n)}{\frac{1}{N}\sum_{k=1}^{N} X_2(k)}\right)^2 \tag{16}$$

The second method consists of normalizing the signals by the square root of their averaged

channel energies:

$$E_2 = \sum_{n=1}^{N} \left(\frac{X_1(n)}{\sqrt{\frac{1}{N}\sum_{k=1}^{N} X_1(k)^2}} - \frac{X_2(n)}{\sqrt{\frac{1}{N}\sum_{k=1}^{N} X_2(k)^2}}\right)^2 \tag{17}$$

Both of the above methods are effective for comparing the shape differences between spectra X_1 and X_2. And for both of them, the closer the normalized differences, E_1 or E_2, are to zero, the more similar are the two spectrum shapes.

3.4.2.3 Spectral Cross Correlation

The local, or short time, cross correlation is used to emphasize the local nature of the coherence between two different signals. It is frequently used to determine similarities between varying signals. For our analysis, the spectral cross correlation is based upon the cross correlation $R_{12}(n, m)$ of two signals $X_1(n)$ and $X_2(n)$ defined by:

$$R_{12}(m) = E_n[X_1(n)\, X_2(n+m)]; \tag{18}$$

where E_n is the expectation over n.

The energy channel, or position of the cross correlation peak, is typically used to estimate the shift between the main carpet spectra peaks, which are the Compton peaks for XRF raw carpet spectra. If the peak position of the cross correlation between two XRF spectra X_1 and X_2 is zero, the Compton peaks are perfectly aligned at the same channel. If not, it implies an imperfect alignment or even calibration or instrumentation problems. After the instrument is successfully calibrated, a value of less than or equal to two should be obtained for the cross correlation peak position m.

When the XRF spectra are shifted by m, the normalized cross correlation, or spectral cross correlation, provides an amplitude independent measure of the spectrum shapes similarity:

$$\gamma_{12}(m) = \frac{R_{12}(m)}{\sqrt{R_{11}(0)\, R_{22}(0)}} \tag{19}$$

For signals of length K (with K being an odd number) centered at 0, the spectral cross

correlation is estimated by:

$$R_{12}^{K}(m) = \sum_{n=-\frac{K+1}{2}}^{\frac{K+1}{2}} X_1(n)\, X_2(n+m) \tag{20}$$

$$\gamma_{12}^{K}(m) = \frac{R_{12}^{K}(m)}{\sqrt{R_{11}^{K}(0)\, R_{22}^{K}(0)}}\ , \tag{21}$$

and the closer to unity $\gamma_{12}^{K}(m)$ is the more similar spectrum X_1 is to spectrum X_2 and vice versa.

3.4.2.4 Shape Comparison

The last method used for data analysis and spectra comparison is a vectorial product between two spectra data sets normalized by the product of their energies. Within a specific window of length N, it consists of (1) multiplying each channel count of the first spectrum, X_1, by each channel count of the second spectrum, X_2, (2) adding those results up and (3) normalizing the whole by the product of their energies:

$$D_{Shape} = \frac{\sum_{n=1}^{N} X_1(n)\, X_2(n)}{\sqrt{\sum_{n=1}^{N} X_1(n)^2}\sqrt{\sum_{n=1}^{N} X_2(n)^2}} \tag{22}$$

This measure gives a sense of the similarity between the spectrum shapes. Specifically, this method is closely related to the Spectral Cross Correlation assuming that $m = 0$. This assumption is reasonable since, as has been mentioned in previous section, the cross correlation peak position is usually always close to zero ($\pm$ two channels) for a calibrated instrument.

CHAPTER IV

RESULTS

4.1 Characterization of the instrument performance

This section is about characterizing the KeyMaster, Tracer II ^{TM}, portable XRF instrument used for all of the measurements. It is expected that the characterization results will be of great interest later for further work with this instrument, and that the characterization methods developed will be useful later on with other XRF instruments. Instrument inconsistencies were measured and placed in two general categories: (1) measurement inconsistencies as a function of the ambient temperature in the exit chamber of the XRF instrument near the specimen, and (2) measurement inconsistencies caused by other sources that affected reproducibility of the results. As stated in Chapter 2, measurement results are not consistent above a temperature threshold of about 96 °F for the instrument used in our studies. Even though the Tracer II ^{TM} utilizes cooled detector technology, i.e., the detector is cooled down to −45 °F, the temperature of the ambient air between the specimen and the detector heats up substantially as the instrument X-ray source is activated, and we attributed the heat source to have contributions from the X-ray tube and electronics inside the instrument. Further, as the temperature increases, the sensitivity of the detector is reduced and the spectra become very noisy. This effect has been noticed for both carpet specimens and other specimen types such as metal alloy specimens; however, it is probably more of a problem for carpet specimens because they are much lower in thermal conductivity than metallic specimens and thus do not conduct heat away from the instrument as efficiently.

The inconsistencies due to the loss in detector sensitivity with temperature were separated for other sources by taking a series of measurements well below 96 °F. We next quantified the remaining inconsistencies using metrics discussed in Chapter 3. First, one set of measurements was made from the same spot on a carpet specimen. In order to quantify differences between these measurements, one of the measurements was taken as

a reference or benchmark, and the remaining measurements were compared to it. Results were calculated for the normalized difference metric described in Chapter 3, Section 4 and recalled here in Eq. 23:

$$d_{i,ref}(k) = \frac{\sqrt{(X_{ref}(k) - X_i(k))^2}}{\frac{X_{ref}(k)+X_i(k)}{2}} \tag{23}$$

Because of the positive nature of the data $X_{ref}(k)$ and $X_i(k)$, $d_{i,ref}(k)$ has the following mathematical properties:

$$0 \leq d_{i,ref}(k) \leq 2 \text{ for } 1 \leq k \leq 1024$$

For each of the series measurement compared to its reference, we calculate the accumulated variation and accumulated variation per channel as respectively described in Eqs. 24 and 25:

$$AV_i = \sum_{k=1}^{N=1024} d_{i,ref}(k) \tag{24}$$

$$AV_{Chan,i} = \frac{1}{N} \sum_{k=1}^{N=1024} d_{i,ref}(k) \tag{25}$$

Finally, the greatest difference GD between the accumulated variations of the series of N measurements is calculated via Eq. 26:

$$GD = \frac{\max_{i \in \, series\, measurements}(AV_i) - \min_{i \in \, series\, measurements}(AV_i)}{\frac{1}{N}\sum_{i \in \, series\, measurements} AV_i} \tag{26}$$

The following statements may be made about the value of $d_{i,ref}(k)$ for any energy channel k: (1) when the value of $d_{i,ref}(k)$ is small, approaching zero, it means that the deviation is negligible between the measurements, (2) when the value of $d_{i,ref}(k)$ approaches one, the variations are on the same order as the average of the two measurements, and thus are significant, and (3) when the value of $d_{i,ref}(k)$ approaches or is equal to two, then one of the two measurements has a count equal to zero. The later case often occurs in low count regions at the extreme ends of the energy spectrum, i.e. approximately below channel 60^{th} and above channel 860^{th}. Thus, variations in these regions were not used for the final statistics where the value of $d_{i,ref}(k)$ approached two.

4.1.1 Influence of the ambient temperature on measurement variations

To characterize measurement variations as a function of ambient temperature in the exit chamber of the instrument (below 96 °F), a set of seven different measurements were performed on the same spot of carpet specimen "GT FA011" at temperatures of 81.9 °F, 82.8 °F, 85.5 °F, 88 °F, 90.4 °F, 92.6 °F and 94.6 °F. Spectra were acquired, and variations were compared to the spectrum obtained at the lowest temperature (81.9 °F), which was the reference spectrum for these comparison calculations. The variations of the six subsequent measurements with the reference spectrum are displayed as a function of energy channels for these different temperatures in Figure 19(a) and analysis results are listed in Table 5.

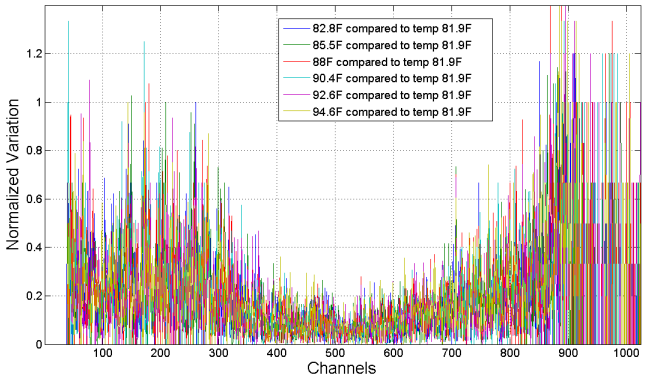

(a) Normalized measurement variations versus channels at several temperatures below 96 °F.

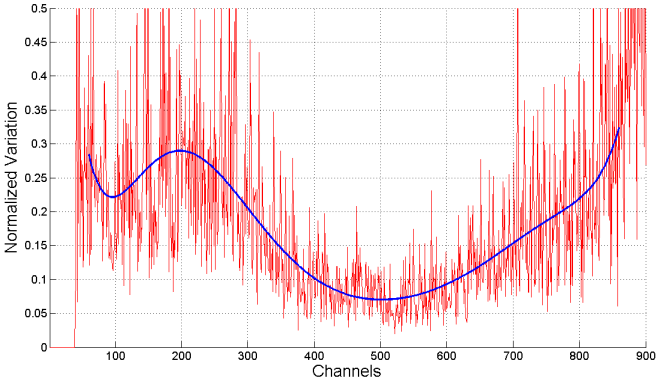

(b) Averaged measurement variations versus channels below 96 °F and of its trend.

Figure 19: Measurement variations for different temperatures below 96 °F.

Several observations may be made for these measurements taken below the temperature threshold of 96 °F: (1) the variations are mostly random and no particular measurement temperature stands out from the others in Figure 19(a), (2) as listed in Table 5, when all the normalized variations are averaged across the energy channels at each temperature, using Eqs. 24 and 25, all the results show about the same degree of random variations, and (3) the greatest difference, obtained via Eq. 26, between the accumulated variations of any of the six measurements compared to the reference spectrum at 81.9 °F shown in Table 5 is 5%.

Table 5: Accumulated variations for measurements at different temperatures compared to the reference spectrum (at temperature 81.9 °F) and calculated using Eqs. 24 and 25.

Measurement	**Accumulated variation** AV	**Accumulated variation per channel** AV_{Chan}
Measurement at 82.8 °F	188.04	0.1836
Measurement at 85.5 °F	189.67	0.1852
Measurement at 88.0 °F	190.55	0.1861
Measurement at 90.4 °F	192.96	0.1884
Measurement at 92.6 °F	187.69	0.1833
Measurement at 94.6 °F	196.48	0.1919

All the curves displayed in Figure 19(a) were averaged together to obtain a single spectrum of measurement variations versus energy channel, and a polynomial was fit to these data to obtain a trend curve. The fit was constrained to channel numbers between 60 and 860 and results are shown in Figure 19(b). Channels lower than 60 and greater than 860 had several zero and low count values in reference spectrum $d_{i,ref}$, thus these channels were not used for the curve fit. The coefficients for this trend curve are listed in Table 6 and given by Eq. 27:

$$Y = a_n \left(X - X_{center}\right)^n + a_{n-1} \left(X - X_{center}\right)^{n-1} + ... + a_1 \left(X - X_{center}\right) + a_0 \qquad (27)$$

For each channel X, the residual $r(X)$ is defined as the difference between the data to fit and the value of the polynomial at this particular channel X as explained by Eq. 28:

$$r(X) = data(X) - Y(X) \qquad (28)$$

For a polynomial fit, the sum of squares of the residuals, shown in Eq. 29, is a good metric for quantifying the way of showing how good the fit is:

$$\sum_{X=n1}^{n2} r^2(X) \tag{29}$$

where $n1$ and $n2$ are the first and last channel indices where we fit the data.

Table 6: Characteristics of the polynomial fit of the averaged spectral variations between channel 60 and 860 for the temperature measurement series.

Degree (n)		**First channel (n1)**		**Last channel (n2)**		**Center channel (X_{center})**			
8		60		860		460			
Coefficients	a_8	a_7	a_6	a_5	a_4	a_3	a_2	a_1	a_0
	0.0152	-0.0152	-0.0604	0.0774	0.0128	-0.0732	0.1708	-0.0550	0.0749

4.1.2 Tests of measurement reproducibility at the same carpet position

To characterize the reproducibility of our measurements, the same method was used as in the previous section where the influence of temperatures below 96 °F was tested. A set of eight measurements were made at the same spot on carpet "GT FS014". Each measurement was taken at a temperature of 83 °F (± 1 °F). As mentioned previously, the portable XRF instrument heats up when the X-ray tube is active, and to make sure that all measurements were made within the target temperature range, all measurements were separated in time by at least four hours to allow the XRF instrument to cool down to ambient laboratory temperature between measurements.

Count variations are displayed as a function of channels for all the measurements at the same carpet position in Figure 20(a). "M1" was the first measurement taken and this was the reference measurement X_{ref} to which all the other measurements are compared. "M2" was the second measurement taken after four hours, "M3" was the next, etc... Each spectrum for these measurements, i.e., "M2" through "M8", was compared to "M1". The resulting variations versus energy channel were averaged over channel numbers 60 through 860 and the results are listed in Table 7.

As was the case for the temperature influence testing, three similar observations can be made, (1) no particular measurement set stands out within these comparisons as being

substantially different, (2) all the averaged count variations calculated using Eqs. 24 and 25 and shown in Table 7 are similar, and (3) the greatest difference, obtained via Eq. 26, between the accumulated variations of any of the seven measurements compared to the reference spectrum from measurement "M1" shown in Table 7 is 17%.

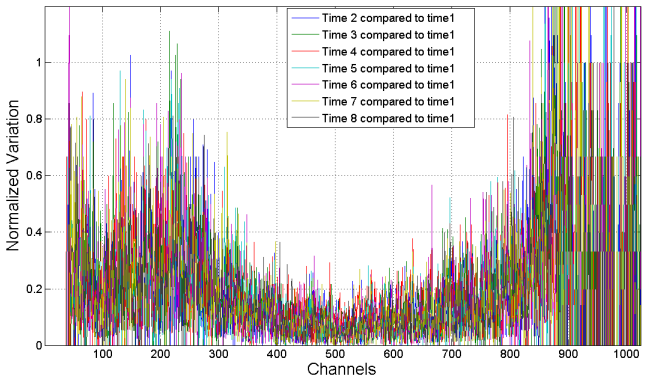

(a) Normalized count variations versus energy channels for different measurements taken after below 83 °F (± 1 °F). M1, the first measurement in the series, is taken as the reference spectrum.

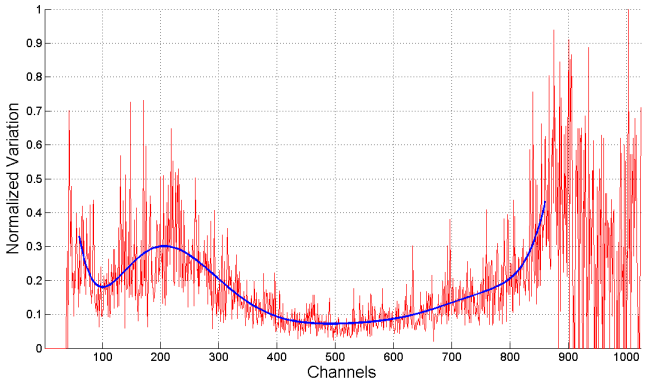

(b) Averaged count variations for measurement reproducibility measurements.

Figure 20: Spectrum variations from carpet specimen "GT FS014" for measurements made at the same position at different times.

This greatest difference, calculated via Eq. 26, between the accumulated variations of the different measurements compared to their reference spectrum of 17% is greater than the 5% value that we obtained in Section 4.1.1 when we tested the influence of temperature

on measurement variations. This means that, even though Tables 5 and 7 look similar, when testing the dwell time effect between measurements on measurement variations, the difference between the lowest and the greatest accumulated measurement variation is more important than when testing the influence of the temperature. One possible explanation is that the temperature measurement series was taken with a wait time of a few minutes between measurements; whereas, the results presented in this section were taken with wait times in the range from four hours to six hours between successive measurements. Thus, we may interpret that the effect of temperature changes, when below a temperature threshold of 96 °F, has a lesser influence on measurement variations than long dwell times between successive measurements.

Table 7: Normalized and accumulated count variations for a series of measurements made on carpet "GT FS014" at different times compared to the reference spectrum M1 and calculated using Eqs. 24 and 25.

Measurement	**Accumulated variation** AV	**Accumulated variation per channel** AV_{Chan}
Measurement M2	205.10	0.2003
Measurement M3	217.04	0.2120
Measurement M4	203.20	0.1984
Measurement M5	190.04	0.1856
Measurement M6	195.55	0.1910
Measurement M7	189.42	0.1850
Measurement M8	186.42	0.1820

As was done previously, all the measurement sets of this section were averaged and a trend curve was fit to the results as a function of energy channel. The trend curve is shown in Figure 20(b). Also as before, a polynomial was used to fit the data shown in Figure 20(b) between energy channel numbers 60 and 860. For this case, the best fit was obtained with an eight order polynomial as expressed in Eq. 30 and with the coefficients listed in Table 8.

$$Y = a_n \left(X - X_{center}\right)^n + a_{n-1} \left(X - X_{center}\right)^{n-1} + ... + a_1 \left(X - X_{center}\right) + a_0 \qquad (30)$$

For each channel X, the residual $r(X)$ is defined as the difference between the data to fit and the value of the polynomial at this particular channel X as explained before by Eq. 28. When testing the influence of a dwell time between measurements, the computed value of the sum of squares of the residuals, from Eq. 29, is 5.23. This value of 5.23 is smaller than the value of the sum of squares of the residuals obtained when testing the influence of temperature and which was equal to 6.91. Quantitatively, this means that the curve fit is

better than the one obtained when testing the influence of the temperature below 96 °F on measurement variations.

Table 8: Characteristics of the polynomial fit to the count variations between channel 60 and 860 for different measurement times at the same spot on carpet "GT FS014".

Degree (n)		**First channel (n1)**		**Last channel (n2)**		**Center channel (X_{center})**			
8		60		860		460			
Coefficients	a_8	a_7	a_6	a_5	a_4	a_3	a_2	a_1	a_0
	0.0318	-0.0269	-0.1349	0.1443	0.1096	-0.1723	0.1308	-0.0272	0.0741

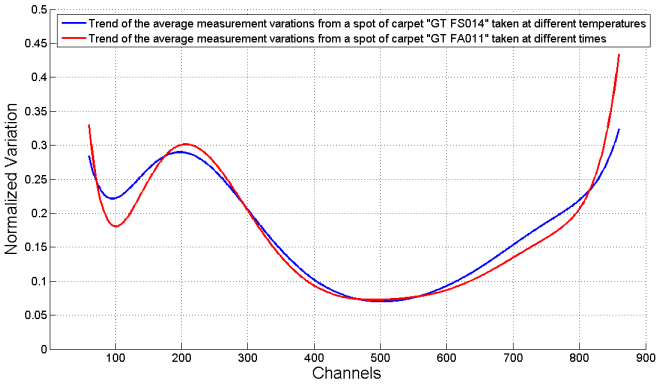

Figure 21: Measurement variation trends versus energy channels for both the temperature and time measurement series.

As shown in Figure 21, neither a temperature below 96 °F nor measurements done at different times have a significant affect on the fitted trend lines. Specifically, both trend lines are about the same magnitude and shape. Thus, we conclude that these fitted trend lines are typical of what one should expect for measurements made with the KeyMaster Tracer II ^{TM} portable XRF instrument in a laboratory environment.

Summary of test results: (1) the trends obtained for the measurement variations from the two tests are similar and (2) the accumulated variations from measurements taken at the same carpet location have the greater affect on measurement reproducibility than the temperature effect.

4.2 Characterization of measurement consistency for carpets

4.2.1 Comparison of measurement consistency with the instrument performance

Both temperature and measurement dwell time affected the reproducibility of spectra obtained from the KeyMaster Tracer II ^{TM} as was shown in the above reported studies. Next, we characterized measurement variations from several different spots on a carpet specimen that, from its visual appearance, is expected to be uniform.

These measurements were made at several different locations of carpet specimen "GT AA007". Note that this is a different carpet specimen than the two used for the temperature and measurement time test series, but the same analysis methods are used to study the measurement variations in this section.

Count variations are displayed as a function of channels for all the measurements at different carpet spots of carpet "GT AA007" in Figure 22(a). The measurement taken at the first spot is the reference measurement X_{ref} to which all the other measurements were compared. The other measurements from four other locations of the carpets are compared to the first one. The resulting variations versus energy channels were averaged over channel numbers 60 through 860 and the results are shown in Table 9.

Table 9: Accumulated count variations for measurements at different positions on carpet specimen "GT AA007" compared to the reference spectrum taken at the first measurement point.

Measurement	**Accumulated variation** AV	**Accumulated variation per channel** AV_{Chan}
Measurement at spot 2	207.4106	0.2025
Measurement at spot 3	195.6374	0.1911
Measurement at spot 4	195.4772	0.1909
Measurement at spot 5	193.7275	0.1892

As shown in Figure 22(b), variations were computed from all the measurement sets, these variations were averaged using Eqs. 24 and 25 and a trend curve was fit as a function of energy channel. Also as before, a polynomial was used to fit the data as shown in Figure 20(b) between energy channels 60 and 860. The best fit was obtained with a eight order polynomial which coefficients are listed in Table 10 and computed value of squares of the

residuals, expressed by Eq. 29, is 5.92. As shown in Figure 23, this trend qualitatively matches with the trends obtained for characterization of the temperature and measurement time effects.

Table 10: Characteristics of the polynomial fit to the count variations between channel 60 and 860 for measurements at different spots on carpet "GT AA007".

Degree (n)		**First channel (n1)**		**Last channel (n2)**		**Center channel (X_{center})**			
8		60		860		460			
Coefficients	a_8	a_7	a_6	a_5	a_4	a_3	a_2	a_1	a_0
	0.0138	-0.0199	-0.0366	0.1024	-0.0479	-0.1169	0.1905	-0.0292	0.0700

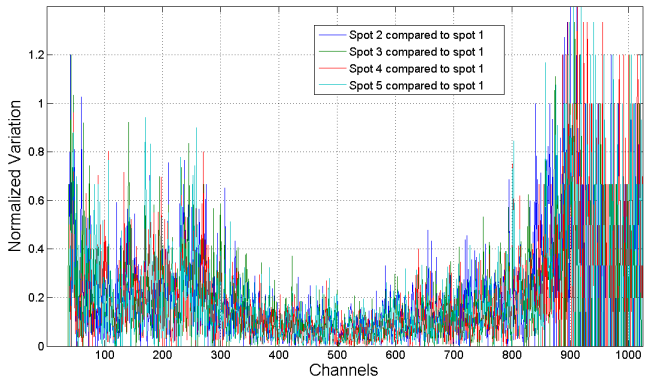

(a) Measurement variations versus energy channel at different spots of carpet "GT AA007".

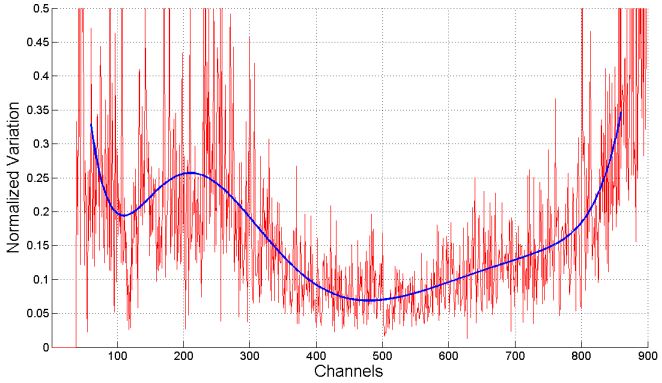

(b) Average measurement variation with a fitted trend line drawn in blue for different spots of carpet "GT AA007".

Figure 22: Measurement variations from different spots of carpet "GT AA007" with average and trend values.

And, as we compare the value of the sum of the squares of the residuals, we notice that a value of 5.92 obtained when testing the influence of carpet uniformity on measurement variations is (1) slightly bigger than the one of 5.23 obtained when testing the influence of a dwell time between measurements and (2) slightly smaller than the one of 6.91 when testing the influence of the temperature below 96 °F. By quantitatively comparing those three results, we deduce that the polynomial fit obtained when testing the influence of carpet uniformity on measurement variations is (1) slightly worse than the one obtained when testing the influence of a dwell time between measurements and (2) slightly better than the one obtained when testing the influence of the temperature.

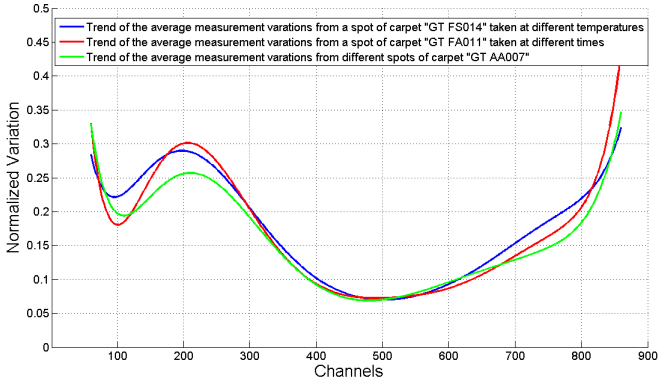

Figure 23: Comparison of the three different trend curves for measurements from the temperature, dwell time and carpet consistency test results channels.

As was the case for the temperature and the measurement dwell time tests, a similar set of observations were made: (1) no particular measurement set stands out within these comparisons as being substantially different, (2) all the averaged count variations shown in Table 9 are similar, and (3) the greatest difference, obtained via Eq. 26, between the accumulated variations of any of the four measurements compared to the reference spectrum taken from the first carpet location shown in Table 9 is 6.9%.

In that case, this greatest difference of 6.9% is closer to the 5% value that we obtained when we tested the influence of temperature on measurement variations, than to the 17%

value, that we obtained when we tested the influence of dwell time on measurement variations. Like the temperature measurement series, the above results were taken with a wait time of a few minutes between measurements; whereas, the results from the dwell time measurement series were taken with wait times in the range from four hours to six hours between successive measurements. Thus, qualitatively we conclude that the effect of temperature changes on measurement variations are almost as important as the effect of carpet uniformity but not as important as the effect of long dwell times between measurements.

4.2.2 Comparison of measurement consistency for carpets selected for our database

In this section results are presented for XRF measurements made on 40 separate carpet specimens. The two quantitative metrics $D1_{total}$ and $D2_{total}$ presented in Chapter 3 are used to quantitatively describe measurement consistency for measurements from different locations on a visually uniform carpet,

To use metrics that are independent of energy channels, as described by equations 31 and 32, we use averages of the metrics $D1_{total}$ and $D2_{total}$ over the energy channels.

$$\frac{1}{N}\sum_{n=1}^{N=1024} D1_{total}(i,n) \tag{31}$$

$$\frac{1}{N}\sum_{n=1}^{N=1024} D2_{total}(i,n) \tag{32}$$

Results for the 40 carpet specimen database are listed in in Table 11. A strong correlation exists between metrics $D1_{total}$ and $D2_{total}$, which were used to quantify differences between measured spectra. The correlation coefficient between these two is equal to 0.847. Recall, $D1_{total}$ characterizes the absolute count difference between each measurement of a same carpet, $D2_{total}$ describes the normalized average standard deviation for one set of measurements on the same carpet.

As shown in Table 11, results for measurement consistency obtained with the two metrics $D1_{total}$ and $D2_{total}$ fall into the following ranges of values: [59.25,106.93] respectively, and [14.67,23.85]. The standard deviations for these metrics are 11.8×10^{-3} and 1.98×10^{-2} respectively, which represent 15% and 11% of their respective mean values. This means

that, regardless of the carpet specimen, the consistency of measurements from different locations is close. From these test results we conclude that the carpet preparation procedure was effective for producing consistent results from all the uniform carpet specimens.

Table 11: Consistency of the measurements of the 40 carpet specimen database using the two quantitative metrics $D1_{total}$ and $D2_{total}$.

Carpet specimen	$\frac{1}{N}\sum_{n=1}^{N=1024} D1_{total}(i,n)$ $(.10^{-3})$	$\frac{1}{N}\sum_{n=1}^{N=1024} D2_{total}(i,n)$ $(.10^{-2})$
GT AA001	59.25	15.18
GT AA007	72.31	16.57
GT AA019	61.49	14.97
GT AA020	59.68	14.67
GT AA021	64.12	16.93
GT AA022	68.20	21.61
GT AA023	64.86	15.80
GT AA024	66.14	18.56
GT AA033	61.27	15.73
GT AA047	69.47	16.68
GT FA003	76.76	17.31
GT FA011	84.92	18.93
GT FA012	106.93	23.85
GT FA016	87.75	18.69
GT FA030	91.88	19.92
GT FA032	82.65	20.20
GT FA034	86.26	18.96
GT FA036	79.33	18.53
GT FA048	77.56	18.76
GT FS002	74.21	17.20
GT FS004	65.66	16.22
GT FS006	83.68	18.52
GT FS008	94.24	20.20
GT FS009	85.24	20.71
GT FS010	87.21	19.08
GT FS013	87.69	19.40
GT FS014	89.68	19.12
GT FS015	93.18	20.64
GT FS018	97.63	21.73
GT FS025	79.30	18.13
GT FS028	90.24	19.32
GT FS029	94.14	20.64
GT FS031	81.49	18.29
GT FS037	85.99	19.60
GT FS039	84.70	19.98
GT FS040	74.08	18.19
GT FS042	86.60	18.79
GT FS044	80.07	18.12
GT FS045	77.78	17.72
GT FS049	97.05	20.63

Additionally, as shown in Table 11, regardless of carpet type, the measurement inconsistencies between different locations are of the same order as the variations observed for the temperature and time measurement series which are shown in Table 5 and 7 respectively.

Further, there is a small observed difference in measurement consistency between carpets

made of Texture “A” and “F”. Specifically, the mean value of the two metrics from Table 11 are 64.68 and 16.67 for carpets with Texture “A” , whereas the corresponding values for carpets with Texture “F” are 85.46 and 19.24. Thus measurements from carpets made of Texture “A”, short-cut pile carpets, are sightly more consistent than carpets with Texture “F” with longer tuft. We attribute this difference to the general difficulty of uniformly brushing the longer tufted Texture “F” carpets and inserting them into a plastic bag for analysis.

4.3 Final algorithm tested on carpets

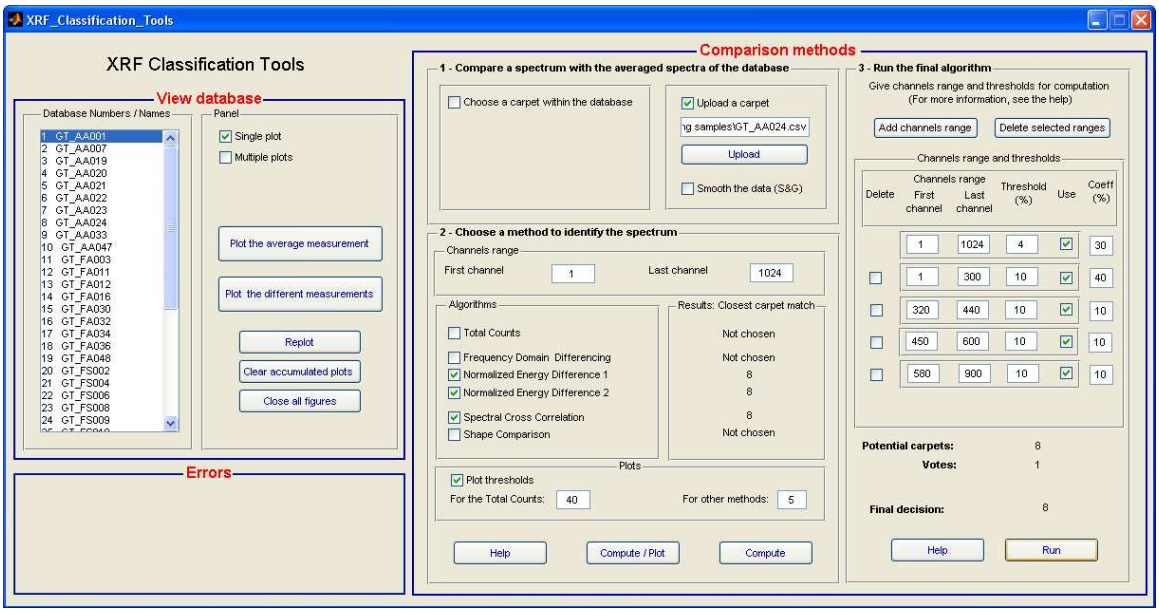

Figure 24: Screen shot of the Matlab GUI implemented developed for data analysis of XRF spectra.

The comparison algorithms summed up by Eqs. 11, 15, 16, 17, 21 and 22 in Section 3.4 were used to classify members of a 40 carpet sample database using XRF measurements. The goal was to identify various carpet types solely from XRF measurements at several locations on each carpet. To expedite data analysis steps, the Matlab Graphical User Interface shown in Figure 24 was implemented to view and interpret the data, as well as to run the final algorithm explained in Section 4.3.1.2. The objective of the algorithms is to match an XRF carpet measurement with the average of measurement values stored in the database for the

actual carpet. Data for each carpet in the database was obtained from five individual XRF measurements acquired from several positions on the carpet. The algorithms explained in Chapter 3 provided the basis for the final database matching.

4.3.1 Final algorithm and methodology

4.3.1.1 Algorithms used

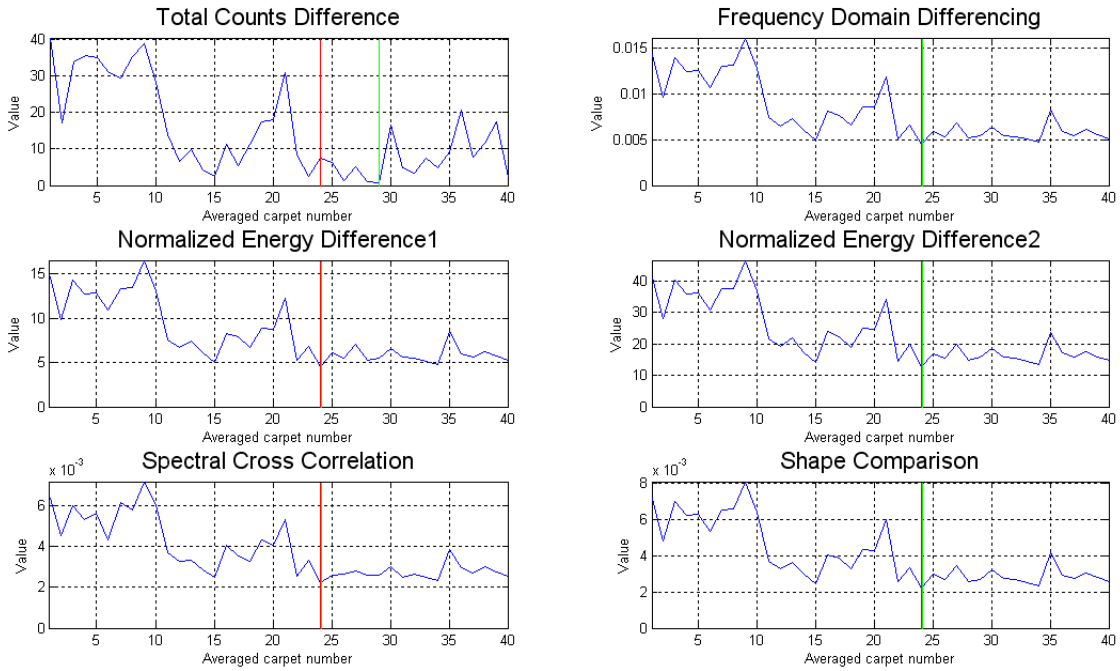

Figure 25: Results of the comparison, within energy channels 1 to 1024, between a new XRF measurement from carpet "GT FS009" and stored database measurements using the various comparison algorithms. The green and red vertical lines represent, respectively, the number of the closest database measurement and the actual carpet number for carpet specimen "GT FS009".

The absolute and relative comparison algorithms, explained in Chapter 3, were tested with different measurements acquired from all specimens represented in the database. These specifically include metrics $D_{TotalCounts}$, E, E_1, E_2, γ_{12} and D_{Shape}. For the comparison methods "Spectral Cross Correlation" and "Shape Comparison", the metrics γ_{12} and D_{Shape} are scaled and offset so that values are close to zero if spectra are similar, which consisted of subtracting the normalized metrics from unity to get the following new metrics: $1-\gamma_{12}$ and $1-D_{Shape}$. Thus, the closer these scaled metrics are to zero, between an XRF measurement

and an averaged database measurement, the better is the match to a carpet in the database.

Comparisons can be made on an absolute basis or a relative basis. For example, Figure 25 shows the results for comparing a new measurement from carpet "GT FS009" to all the other carpets in the database. For this comparison, the best match corresponds to the itself, i.e. the actual carpet (database number 24 for carpet "GT FS009"). For the absolute comparison, the best match corresponds to the carpet corresponding to database number 29.

As displayed in Figure 25, using the different relative comparison algorithms to match an XRF carpet measurement with the averaged database measurements gives similar results. That is why, for the final decision algorithm, only one metric is used for relative shape comparison of the XRF spectra. Specifically, the "Shape comparison" metric described by Eq. 22 is sufficient and was used for the final comparison of spectrum shapes.

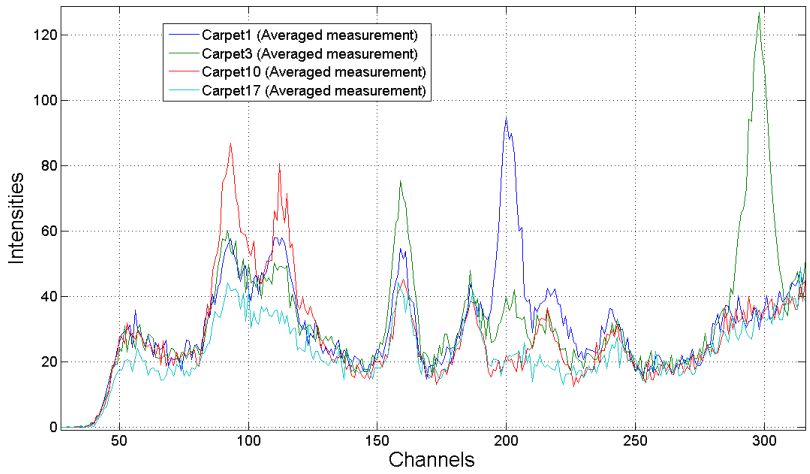

Figure 26: XRF carpet spectrum details of four averaged spectra for selected low energy channels.

An important parameter when implementing any of these comparison algorithms is the energy channel range or channel window used for the spectrum comparison. Whereas using the entire energy channel range allows a complete data comparison, using specific channel intervals may emphasize the differences between carpets within characteristic energy channels. For instance, comparison of two spectra within energy channels ranging from 1

to 300, i.e. energies ranging from 0 to 7.5 keV, emphasizes differences in peaks of low energy transition elements such as iron (Fe), nickel (Ni) and copper (Cu). In Figure 26, examples of the significant differences of four carpets for low energy channels are displayed for the averaged measurements. Similarly, comparison of spectra within energy channels ranging from 450 to 600, i.e. energies ranging from 11.3 to 15 keV, compares spectra near the Compton and silver (Ag) peaks, which originate from the primary X-ray beam and the silver source of the instrument respectively. Our final choice of energy channel ranges is explained in the next section.

4.3.1.2 Final algorithm model

To determine which database specimen is the best match to a specimen being analyzed, it is assumed that the specimen which matches the greatest number of energy ranges has the highest probability of being the true match or a least very similar in spectra characteristics. Thus, the more energy ranges are used in the comparison, the more probabilities are improved. For this study, typically five energy ranges were used, one near the Compton peak and others near known constituents that might be in specific carpets, but not near peaks of taggant elements. Recall one anticipated use of this technology is to measure the concentrations of taggants which may be placed in carpets to determine process chemistry concentrations. Measurements from different energy ranges were quantified using a voting scheme as is often used in pattern-matching algorithms for computer-aided identification [17], [18] and [19]. The voting scheme relies on three different aspects which maximize our chance to match the XRF spectrum measurement with the database averaged measurement representative of the actual carpet: (1) results combinations from different energy channel ranges, (2) use of thresholds to set good results confidence and (3) weighting the different results to give more or less importance to specific individual results

The final algorithm is based on a voting scheme and consists of four major consecutive steps which are shown in Figure 27: (1) applying a relative spectrum comparison with one of the algorithms explained in the previous section within different characteristic energy channel ranges, (2) using thresholds and combining results to get sets of potential carpet

matches for specific energy channel ranges, (3) ranking proportional votes for the potential carpets on each energy channel range, and (4) combining the voting results of the different energy channel ranges by weighting the results from the different channel ranges.

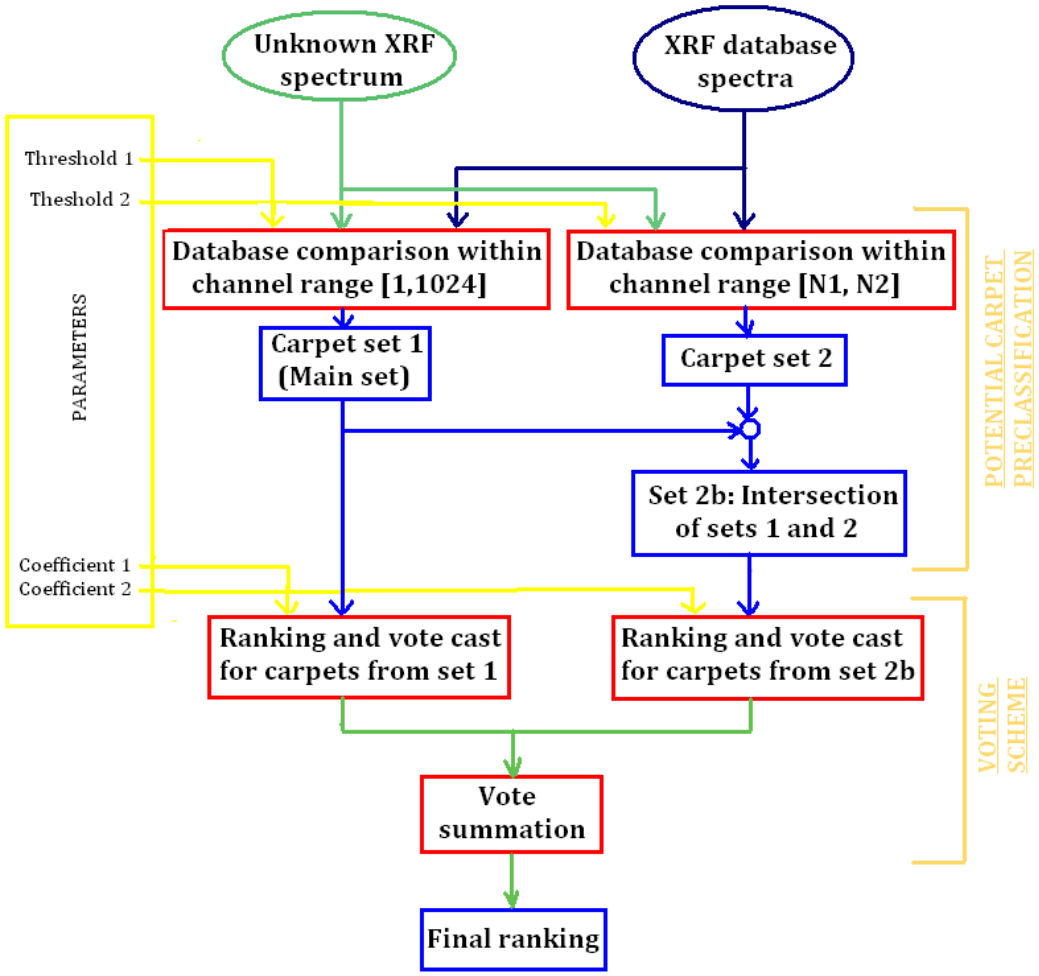

Figure 27: Model implemented for the final algorithm for different channels ranges of interest.

Steps of the final algorithm are detailed in this paragraph. First, relative spectrum comparison is made between a XRF measurement from a new carpet and stored database measurements. This comparison is quantified using the "Shape Comparison" metric for five different specific energy channel ranges, and these are 1^{st} to 1024^{th}, 1^{st} to 300^{th}, 320^{th} to 440^{th}, 450^{th} to 660^{th} and 580^{th} to 990^{th}.

Second, for each of these different energy channel ranges, a set of potential database carpets is inferred, for which the "Shape Comparison" metric is below a certain threshold.

The energy channel range from the 1^{st} to the 1024^{th} channel, which contains all the information of the XRF spectra, is weighed to be the most significant energy channel range. As a consequence, for each of the other channel ranges, the potential database matches are dismissed if the match is not sufficiently close for the total energy range. Certainly this voting procedure may be adjusted later when taggants are measured, then probably the total range would be used as the most important one with holes in the range to remove the influence of taggant peaks which would be expected to vary with taggant concentration.

Third, results obtained for each energy channel range are ranked so that each carpet gets a vote normalized to 1 which is proportional to its rank. Within a result set of N specimens, the specimen ranked first receives a vote equal to 1, the one ranked second receives a vote equal to $\frac{N-1}{N}$, etc...

Finally, for each of the potential candidates within the different energy channel ranges a weighted averaged vote is computed from the coefficients assigned to the various energy channel ranges. From there, the potential carpets are ranked according to the average of the weighted votes and the final vote percentages are normalized to one. Finally, the carpet with the highest vote is the most probable match.

Table 12: Energy channel ranges and corresponding parameters used for the final voting algorithm.

Energy channel range number	**First channel (n1)**	**Last channel (n2)**	**Threshold (%)**	**Coefficient**
1	1	1024	5%	30
2	1	300	10%	40
3	320	440	10%	10
4	450	600	10%	10
5	580	900	10%	10

All the parameters used for the final algorithm are shown in Table 12. And, as an example, consider the results of the potential matching carpets on the different energy channel ranges obtained for a certain database carpet and displayed in Table 13. Consider that (1) as shown in the second column of Table 13, there are respectively three, four, seven, six and eight potentially matching carpets for each respective channel range and (2) as shown in third column of Table 13, the database carpet is ranked respectively as the second, third, first, fifth and sixth best potentially matching carpet for each channel range. Then, votes for this carpet for each of the channel results are deduced in the fourth column.

Finally, using the weighting coefficients given in Table 12, the carpet casts a final vote equal to:

$$\frac{30 \times \frac{2}{3} + 40 \times \frac{1}{2} + 10 \times 1 \times \frac{1}{3} + 10 \times \frac{3}{8}}{30 + 40 + 10 + 10 + 10} = 0.5708 \tag{33}$$

Table 13: Fictive results for a database carpet and corresponding votes cast for each of the comparison energy channel ranges.

Energy channel range number	Number of potentially matching carpets	Rank of carpet "A" within the potentially matching carpets	Vote cast
1	3	2^{nd}	2/3
2	4	3^{rd}	1/2
3	7	1^{st}	1
4	6	5^{th}	1/3
5	8	6^{th}	3/8

4.3.1.3 Methodology for choosing final algorithm parameters

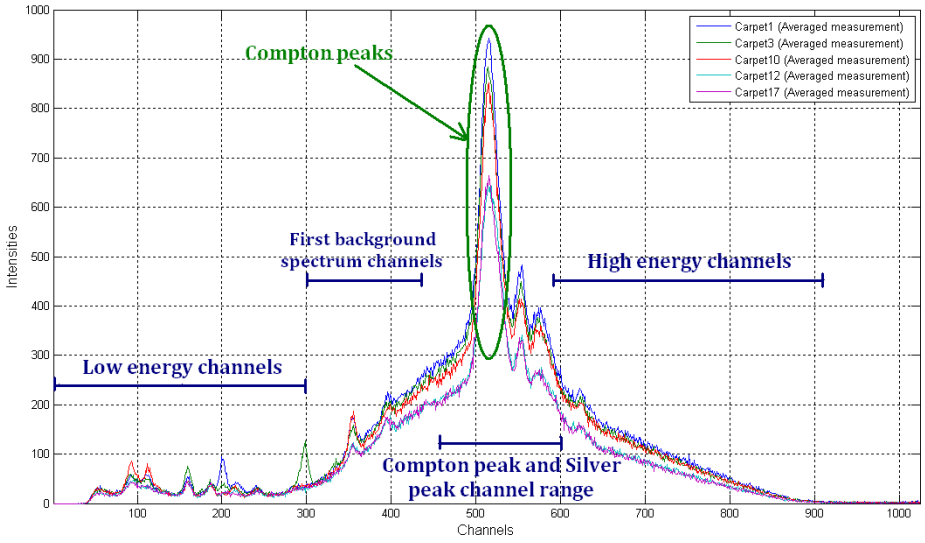

Figure 28: Methodology for choosing different characteristic energy channel ranges for the final algorithm.

In this section, a methodology to choose suitable parameters for the final algorithm is proposed. We recall that the parameters used for the final algorithm are: (1) the specific energy channel ranges or channel windows within which the spectra are compared, (2) the thresholds below which a carpet is considered as a potential matching carpet and (3) the

weighting coefficients to assign to each one of the energy channel ranges. Parameters for all three of the above factors are largely chosen for empirical reasons. As shown in Figure 28 and explained before, the five most significant energy channel ranges are chosen by visually comparing the XRF spectra and choosing the most representative XRF spectrum characteristics to emphasize comparison between carpets. Then, the selection of a threshold below which a carpet is considered to be a potential match is made so that a sufficient number of carpets will be considered as potential matching carpets. Finally, the choice for the value of the coefficients assigned to each one of the different energy channel ranges for the final voting scheme depends upon how confident we are in the results of each energy channel range. The more confident we are in the results obtained from a channel range and the greater its significance for a specific carpet, then the greater its weight should be.

4.3.2 Database consistency check

The first validation consisted of testing the efficacy of our algorithms, in terms of database matching, using each different measurement from the database and comparing it with the average of the stored measurements. This test is certainly biased since the test measurements are part of the information in the database. However, it is a good first validation test to determine the efficacy of our comparison and classification algorithms. For this evaluation all the metrics from the five energy ranges were computed and the one with the lowest value was used as the criterion to select a carpet from the database, instead of using a voting scheme. Results showed that the measurements match very well: 197 database measurements out of 200 (5 measurements for 40 carpets) matched perfectly with the average of the measurements stored in the database for selecting the actual carpet. These results indicate that the individual measurements from each carpet, recall there are five, are mostly all consistent with the spectrum obtained by averaging the five individual measurements from each carpet.

4.3.3 Results from new XRF measurements

The second validation test consists of acquiring a second independent set of measurements from the carpet samples that were used to construct the original database. The classification

algorithms were then used to determine if each carpet sample could be matched to the actual carpet stored in the database. This second measurement set was acquired a week after the original database measurements. For each carpet, a measurement of a random spot is acquired after having prepared the carpet by brushing it unidirectionally and inserting it into a plastic bag. This preparation procedure is explained in Chapter 2. When spectra are compared within energy channels ranging from 1 to 1024, and when again using the closest metric value to zero as a matching criterion instead of the final voting algorithm, 18 out of 40 carpets matched with the actual carpets from the database. This is fewer matches than were found for the database consistency check, but this is expected since these are new measurements which are not contained in the original database.

The voting scheme discussed previously was next implemented to improve the carpet matching statistics instead of using just the metric with the lowest value for the match comparison. For the 40 carpet measurements, independent from the database measurements, results obtained with the final database matching algorithm explained in section 4.3.1 are compared with the actual carpet. Specific parameters (such as threshold and coefficient) for each energy channel range used in Section 4.3.1.2 for the final algorithm and its voting scheme have been given in Table 12. Results from the final algorithm are presented in Table 14. The numbers of the final potential carpets and their respective votes for each one of the new measurements are listed in the second and third column of the table. The true matches, underlined and highlighted in blue in the table, are actually very close to the actual match results obtained with the final algorithm. Except for one of the new measurements from one carpet samples, all the other measurements have their actual carpets as a potential match. For 20 out of the 40 carpets, the actual carpet has the best vote among the potential carpets. When the true carpet was not matched as a first choice, its rank among potential matches is shown in the third column of Table 14, with the best match listed on the left side of the column.

In this section, final algorithm developed for carpet database matching purposes and a methodology to choose its appropriate parameters have been been presented. To test the different algorithms, two different sets of measurements have been used: (1) the database

measurement set and (2) a set of measurements that were independent from those used for constructing the original database.

Table 14: Results of final algorithm for testing measurements - For each testing measurement, potential matching carpets are displayed with their corresponding votes from the voting scheme. Results for the true match are highlighted and underlined in blue.

Carpet number	Numbers of potential carpets	Respective votes (normalized to 1)
1	1	0.9
2	2	0.9
3	3 - 4 - 9	0.77 - 0.4 - 0.33
4	3 - 4 - 5	0.57 - 0.97 - 0.22
5	4 - 5 - 7 - 21	0.88 - 0.59 - 0.33 - 0.2
6	4 - 5 - 6 - 21	0.55 - 0.62 - 0.58 - 0.41
7	5 - 7 - 10	0.67 - 0.72 - 0.37
8	1 - 8	0.4 - 0.9
9	3 - 9	0.8 - 0.65
10	5 - 7 - 10	0.57 - 0.23 - 0.8
11	11 - 12 - 18	0.77 - 0.58 - 0.4
12	11 - 12 - 14 - 18 - 38	0.3 - 0.47 - 0.84 - 0.56 - 0.38
13	23	0.9
14	14 - 30 - 31 - 36	0.8 - 0.5 - 0.3 - 0.4
15	15	1
16	12 - 16	0.45 - 0.8
17	17	0.9
18	18 - 38	0.4 - 0.9
19	12 - 18 - 19	0.75 - 0.53 - 0.57
20	17 - 20 - 35	0.63 - 0.53 - 0.63
21	21	0.9
22	22 - 24 - 26 - 28 - 33 - 34 - 37	0.69 - 0.43 - 0.8 - 0.39 - 0.54 - 0.18 - 0.42
23	13 - 23	0.8 - 0.4
24	15 - 24 - 33 - 34	0.47 - 0.9 - 0.43 - 0.2
25	25 - 31 - 36	0.67 - 0.67 - 0.27
26	22 - 24 - 26 - 33 - 34 - 37	0.6 - 0.51 - 0.71 - 0.39 - 0.67 - 0.17
27	25 - 27 - 31	0.97 - 0.6 - 0.33
28	22 - 24 - 26 - 28 - 29 - 33 - 34	0.52 - 0.37 - 0.7 - 0.68 - 0.32 - 0.49 - 0.23
29	22 - 29	0.45 - 0.9
30	11 - 12 - 18 - 30 - 32 - 37 - 38 - 39	0.6 - 0.23 - 0.78 - 0.43 - 0.74 - 0.36 - 0.3 - 0.11
31	25 - 31	0.4 - 0.9
32	32 - 34 - 36 - 40	0.63 - 0.48 - 0.33 - 0.62
33	15 - 24 - 33 - 34 - 37	0.54 - 0.74 - 0.64 - 0.28 - 0.5
34	15 - 22 - 24 - 26 - 33 - 34 - 37 - 40	0.95 - 0.66 - 0.69 - 0.56 - 0.61 - 0.4 - 0.16 - 0.32
35	17 - 20 - 35	0.43 - 0.5 - 0.67
36	25 - 27 - 36	0.63 - 0.65 - 0.62
37	26 - 33 - 37 - 38	0.85 - 0.7 - 0.4 - 0.3
38	12 - 18 - 38	0.87 - 0.57 - 0.47
39	15 - 22 - 26 - 33 - 34 - 37 - 39	0.45 - 0.78 - 0.75 - 0.39 - 0.34 - 0.55 - 0.24
40	22 - 24 - 32 - 34 - 40	0.61 - 0.36 - 0.54 - 0.68 - 0.27

The database measurement set has been used as an appropriate first set to test our data analysis algorithms: these database matching results have showed that the algorithm is effective with respect to classifying carpet types. Then, using the final voting scheme

algorithm with specific weight parameters, matching results from the set of the 40 database independent measurements have been computed and following performance statistics for the classification algorithms have been deduced: (1) the probability of getting the true carpet as one of the potential carpet matches is equal to 97.5% and (2) the probability that the true carpet has the highest vote among the potential carpets is 50%. As mentioned before, the new measurements used to test the database were acquired after a long dwell time, about one week, after the original database measurements. For this reason we expect our results for the test measurement set to be less consistent that the original database measurements which were taken with very little dwell time between the five measurements made on each carpet specimen. Specifically, as mentioned in Section 4.1, measurement variations due to a long dwell time are a factor 3 greater than measurement variations due to different locations on the same carpet.

CHAPTER V

CONCLUSION AND RECOMMENDATIONS FOR FUTURE WORK

Three main points have been undertaken in this thesis: (1) set up of a defined procedure for XRF online analysis of carpets, (2) characterization of the performance of the KeyMaster Tracer II ^{TM} portable XRF instrument and (3) classification of carpets using XRF spectra measured from typical carpet samples.

X-ray count versus energy spectra are obtained in a typical measurement using a hand held XRF instrument. Results obtained are a function of several experimental variables which include the X-ray tube voltage, X-ray tube current, and the ambient air temperature of the instrument chamber. The XRF spectra rely on the way the samples are analyzed, i.e. the distance between the X-ray detector and the top fibers and the carpet pre-measurement preparation. Knowing those parameters of influence, a procedure for XRF carpet online analysis has been been proposed. Even though this procedure is a little specific to our XRF instrument, we would recommend to set up a similar procedure to control these different parameters by using our procedure guidelines.

A procedure was established in Chapter 2 and reproducibility and consistency tests were conducted to characterize the consistency of spectra obtained from the KeyMaster Tracer II ^{TM}. These included measurement series to determine (1) temperature sensitivity, (2) the effect of dwell time between successive measurements, and (3) the measurement variations for measurements made at separate positions on a visually uniform carpet specimen. These tests showed that the effect of a large dwell time between measurements causes variations that are approximately a factor 2 or 3 times variations from test temperature changes, provided that the temperature was kept below 96 °F. Additionally, variations due to a large dwell time between measurements are approximately a factor of 2 greater than measurement variations from different positions on the same carpet, when the carpet is uniform.

Knowing these results, we changed our final measurement procedures to minimize the above spectrum variations. Specifically, measurements are made with a dwell time of several minutes between measurements instead of hours between measurements, i.e., just sufficient in length to keep the exit chamber of the XRF instrument below a temperature of 96 °F.

Finally, to help in automating the XRF calibration process for analyzing XRF raw carpet spectra, a set of 40 carpet samples was measured and XRF spectra were cataloged in a database to be used for carpet classification purposes. Results from the database matching showed that, when using a new set of testing measurements that were acquired a long dwell time after the database measurements, the matches corresponded to the actual carpet specimen in one case out of two. We deduced that the measurement dwell time influence mentioned in Section 4.1 was an important parameter that affected the confidence in the database matching results.

In the thesis, XRF analysis of raw carpets has been studied, and several points can be made: (1) the study provided a basis for checking measurement reproducibility of XRF carpet spectra and for characterizing an XRF instrument accuracy performance, (2) it met goals for setting up a documented final procedure for XRF analysis, and (3) it showed the feasibility of using XRF technology for classifying raw carpets.

This study is also a basis for future work on XRF analysis of carpet spectra, but additional work will be required before online applications can be realized. Specific areas recommended for further development include: (1) working on a way to calibrate and quantify the measurement dwell time effect, (2) automating the energy ranges used as the basis for the voting scheme, (3) adding features to the final algorithm to suppress strong peaks of elements that will be added later as taggants in carpets, and (4) extending the protocol used here for database matching to categories of carpets, rather than just individual carpet samples.

APPENDIX A

MILL CHARACTERISTICS OF THE 49 CARPETS SAMPLES

Table 15: Mill characteristics of the 49 carpets samples.

Sample	Color	Texture	Pile Height	Density	Weight	Backing	Code
GT AA001	401	A	0.13	6646	24	Action	77318
GT AA007	501	A	0.37	3795	39	Action	57003
GT AA019	303	A	0.13	7200	26	Action	77233
GT AA020	101	A	0.14	7200	28	Action	77280
GT AA021	101	A	0.13	7200	26	Action	77281
GT AA022	303	A	0.12	7800	26	Action	77353
GT AA023	501	A	0.12	8400	28	Action	77232
GT AA024	806	A	0.11	9164	28	Action	77360
GT AA033	901	A	0.11	8509	26	Action	77234
GT AA047	746	A	0.14	6686	26	Action	77129
GT FA003	707	F	0.58	1552	25	Action	51404
GT FA011	250	F	0.5	2110	29.3	Action	73593
GT FA012	750	F	0.81	1516	34.1	Action	51395
GT FA016	305	F	0.51	3106	44	Action	51112
GT FA017	402	F	0.21	4800	28	Action	57019
GT FA030	303	F	0.67	2359	43.9	Action	51737
GT FA032	155	F	0.9	1000	25	Action	51799
GT FA034	107	F	0.43	3022	36.1	Action	50543
GT FA036	154	F	0.67	1574	29.3	Action	51033
GT FA048	718	F	0.89	1064	26.3	Action	51738
GT FS002	223	F/A	0.34	3716	35.1	Soft	51717
GT FS004	701	F/A	0.21	6913	40.9	Soft	51568
GT FS005	101	F/A	0.32	4374	39	Soft	51768
GT FS006	101	F	1.03	2045	58.5	Soft	51681
GT FS008	720	F	1.08	1137	34.1	Soft	51432
GT FS009	994	F	1.18	1934	63.4	Soft	59176
GT FS010	610	F	0.58	3755	60.5	Soft	51106
GT FS013	107	F	0.92	1910	48.8	Soft	51019
GT FS014	330	F	0.77	4105	87.8	Soft	51844
GT FS015	773	F	0.96	2558	68.2	Soft	59205
GT FS018	112B	F	2.21	1587	97.4	Soft	51666
GT FS025	121	F	0.8	1840	40.9	Soft	51582
GT FS026	700	F	0.27	6531	48.8	Soft	51647
GT FS027	751	F	0.36	3510	35.1	Soft	51751
GT FS028	505	F	0.62	3681	63.4	Soft	51851
GT FS029	141	F	0.79	2096	46	Soft	51611
GT FS031	701	F	1.18	1248	40.9	Soft	51816
GT FS035	150	F	0.32	4388	39	Soft	51479
GT FS037	600	F	1.06	2153	63.4	Soft	51386
GT FS038	102	F	0.41	3512	40	Soft	51787
GT FS039	121	F	0.38	3316	35	Soft	59219
GT FS040	108	F	0.56	3761	58.5	Soft	51455
GT FS041	800	F	0.3	4618	39	Soft	51608
GT FS042	103	F	1.16	1210	39	Soft	51817
GT FS043	778	F	0.38	3411	36	Soft	51764
GT FS044	714	F	0.81	1560	35.1	Soft	51828
GT FS045	722	F	1.18	1403	46	Soft	51544
GT FS046	305	F	0.37	3892	40	Soft	51774
GT FS049	106	F	0.69	2546	48.8	Soft	51592

APPENDIX B

LIST OF THE SAMPLES FROM THE FINAL DATABASE

Table 16: List of the final database samples with their corresponding numbers.

Carpet sample ID: **Carpet sample number:**	GT AA001 1	GT AA007 2	GT AA019 3	GT AA020 4	GT AA021 5	GT AA022 6
GT AA023 7	GT AA024 8	GT AA033 9	GT AA047 10	GT FA003 11	GT FA011 12	GT FA012 13
GT FA016 14	GT FA030 15	GT FA032 16	GT FA034 17	GT FA036 18	GT FA048 19	GT FS002 20
GT FS004 21	GT FS006 22	GT FS008 23	GT FS009 24	GT FS010 25	GT FS013 26	GT FS014 27
GT FS015 28	GT FS018 29	GT FS025 30	GT FS028 31	GT FS029 32	GT FS031 33	GT FS037 34
GT FS039 35	GT FS040 36	GT FS042 37	GT FS044 38	GT FS045 39	GT FS049 40	

REFERENCES

[1] How xrf works. 2008. http://www.niton.com.

[2] R Scholtz and S Uhlig. Introduction to x-ray fluorescence. 2006.

[3] B Beckhoff, B Kanngieer, N Langhoff, R Wedell, and H Wolff.

[4] R Jenkins, R W Gould, and D Gedcke. *Quantitative X-ray Spectrometry*. Marcel Dekker, New York, 1981.

[5] R Jenkins. *X-Ray Fluorescence Spectrometry*. Wiley John and Sons Inc, second edition, May 1999.

[6] P H Abbott and M J Adams. Strategies for x-ray fluorescence spectra interpretation. Sept 1995.

[7] R E Van Grieken and A A Markowicz, editors. *Handbook of X-ray Spectrometry - Methods and Techniques*, volume 14. New York - Basel - Hong Kong, 1993.

[8] A Savitzky and M J E Golay. Smoothing and differentiation of data by simplified least squares procedures. *Physical Review*, 1964.

[9] S Steenstrup. A simple procedure for fitting a background to a certain class of measured spectra. 1981.

[10] D Wegrzynek, A Markowicz, and A Mendoza Cuevas. Evaluation of the energy-dispersive x-ray spectra of high-z elements using gaussian and voigt peak shape profiles.

[11] L Bennun, E D Greaves, and J J Blostein. New procedure for intensity and detection limit determination in spectral trace analysis: application for trace mercury by txrf.

[12] Summary of pertinent standards and requirements of the $hud/fha\,um44d$. May 2006.

[13] R O Muller. *Spectrochemical Analysis By X-Ray Fluorescence*. Plenum Press - New York - 1972.

[14] H Mark and J Workman. *Statistics in Spectroscopy*. ELSEVIER - Academic Press, second edition, 2003.

[15] J.E. Michaels, Y. Lu, and T.E. Michaels. Methodologies for quantifying changes in diffuse ultrasonic signals with applications to structural health monitoring. *Health Monitoring and Smart Nondestructive Evaluation of Strucutral and Biological Systems IV*, 2005.

[16] J E Michaels and T E Michaels. Detection of structural damage from the local temporal coherence of diffuse ultrasonic signals. *IEEE transactions on Ultrasonics, Ferroelectrics, And Frequency Control*.

[17] K Grauman and T Darrell. Efficient image matching with distributions of local invariant features. November 2004.

[18] G Schindler, M Brown, and R Szeliski. City-scale location recognition. 2006.

[19] Z Arzoumanian, J Holmberg, and B Norman. An astronomical pattern-matching algorithm for computer-aided identification of whale sharks rhincodon typus. *Journal of Applied Ecology*, 2005.